Applicability of large eddy simulations to capture turbulence attenuation in particle-laden channel flows

Naveen Rohilla ⬡, Pradeep Muramulla, and Partha S. Goswami ⬡[*]

Department of Chemical Engineering, IIT Bombay, Mumbai 400076, India

We report a critical assessment on the applicability of the large eddy simulation (LES) technique in predicting turbulence modulation due to the presence of particles with high Stokes numbers. The simulations have been performed for two Reynolds numbers of 3300 and 5600 based on average gas velocity and channel width. An increase in particle loading decreases the turbulence intensity, and at a particular volume fraction, the turbulence collapses due to the catastrophic reduction of turbulence production. It is observed that at low volume fractions, LES models predict the turbulence modulation with high accuracy (>80%) but fail to predict the volume fraction [critical particle volume loading (CPVL)] at which turbulence collapse happens. A detailed analysis shows that an inaccurate prediction of the turbulent energy production is the source of error in CPVL prediction. This is contrary to the usual understanding of the limitation of the LES models in predicting accurate energy dissipation.

I. INTRODUCTION

Particle-laden turbulent flows are ubiquitous in industrial processes such as coal combustion, fluidized bed reactors, pneumatic transport of solid particles, particulate industrial exhaust, etc., and natural processes such as sand and dust storms. A detailed understanding of interactions between gas and particle phase is required to design process equipment with higher and energetically efficient performance. Different length and time scales associated with the turbulent flows make it difficult to understand the interaction between the particle and fluid phases. The dynamics of both phases depend on the flow conditions such as fluid phase Reynolds number, particle inertia, and particle mass loading. The particle-particle and particle-wall interactions also play a significant role in determining the dynamics [1].

In last two decades, a number of numerical techniques have been used to address the issues such as particle clustering at low Stokes number [2,3] and fluid-phase turbulence modulation [1,4–14]. In a few of the earlier studies, the Reynolds averaged Navier-Stokes (RANS) equation has been used to model the fluid phase [15–17]. Such an approach can predict the average properties of both phases. However, fluctuating dynamics are not captured well, which is important in understanding mass and heat transfer processes in gas-solid turbulent flows. Direct numerical simulation (DNS) has also been applied to solve the fluid phase equations. The hard-sphere molecular dynamic simulation strategy has been used to address the particle dynamics in a Lagrangian frame [6,10,14,18–22]. However, the major disadvantage of DNS is that it is computationally very expensive, which restricts its use to low Reynolds number and for a small system size. Even with the advent of the high-speed computing system, it is almost impossible to perform DNS for a system size that is of practical importance. Considering the limitation of RANS in predicting fluctuating dynamics and the

---

[*]psg@iitb.ac.in

computationally expensive nature of DNS, the large eddy simulation (LES) plays an important role in predicting fluctuating dynamics at high Reynolds numbers. In LES, large scale motions which are responsible for turbulent momentum transfer and mixing are resolved, and different closure models are used to model the subgrid scale stresses.

The first LES closure model was proposed by Smagorinsky [23], although it was found to suffer from high dissipation for certain flows such as wall-bounded flows and jet flows. In subsequent studies, different authors have used different values of the Smagorinsky coefficient (C_s) depending on the system geometry [4,24–26]. Canuto and Cheng [27] have discussed the assumptions of the Smagorinsky-Lilly model and reported a decrease in C_s by a factor of 2–3 compared to the theoretical value. The dynamic Smagorinsky model is found to perform better than the Smagorinsky model [28] as the eddy diffusivity is calculated dynamically with the evolution of the flow in the case of the former. Fureby *et al.* [29] have reported that both the models suffer to accurately predict the streak spacing in a turbulent channel flow, although the second moment of the fluid velocity fluctuations is well predicted.

In the case of particle-laden flows, Kuerten and Vreman [30], and Kuerten [31] studied the turbophoresis phenomenon and concluded that the turbophoresis cannot be captured accurately without the particle subgrid scale (SGS) model. Marchioli *et al.* [32,33] found that LES predicts the particle velocity statistics satisfactorily. However, the particle segregation is not predicted well, especially near the wall for a wide range of Stokes numbers. They suggested that introducing the correct level of velocity fluctuations in the particle equation of motion may not be enough to eliminate that discrepancy; a rendering of flow fields might be needed. Marchioli *et al.* [32] and Stolz *et al.* [34] performed the simulation with the approximate deconvolution model (ADM) technique for fine and coarser grids. ADM can recover a portion of the filtered velocity, but it cannot recover the fluctuation modes that are lost in the filtering process [35]. A transport equation for SGS kinetic energy to recover the loss of energy due to filtering did not improve the particle statistics [36]. The particles are less affected by the small scale eddies as the Stokes number increases [37]. A comprehensive assessment of the particle subgrid scale models is performed by Cernick [38]. Marchioli [39] has reviewed the effect of subgrid scale fluctuation on the particle phase statistics and different particle subgrid scale models. From the data available in the literature, it was shown by Marchioli [39] that subgrid scale fluctuations have minimal effect on the particle statistics if the particle subgrid Stokes number based on the subgrid scale fluid time scale calculated at the particle Lagrangian position is greater than 5. It is worth noting that the present study deals with the particles having subgrid Stokes number almost two orders of magnitude higher than the cutoff limit.

A majority of the numerical studies which use LES have used the one-way coupling technique without considering the particle-particle collisions [30,31,33,35–37,39–44]. Therefore, these studies did not address the applicability of LES models on capturing the effect of particle phase on turbulence modulation. The different approaches used in LES have been reviewed by Kuerten [45]. The turbulence modulation has been studied experimentally by Kulick *et al.* [7], Kajishima [8], and Coletti *et al.* [9], and numerically via DNS by Vreman *et al.* [10], Li *et al.* [11], Vreman [6], and Muramulla *et al.* [12]. It has been observed that turbulence modulation depends on different parameters such as Stokes number, particle Reynolds number, mass loading, bulk Reynolds number, etc. In two-way coupled DNS, Battista *et al.* [46] extended the exact regularized point particle (ERPP) method [47] to account for the effect of a wall on the vorticity induced by the inertial particles. The effect of an additional stress term generated due to interphase coupling affects the turbulence intensity. The authors have observed a reduction in the Reynolds stress and increased viscous stress due to an increase in momentum flux toward the wall. Consequently, the drag increases. The effect of feedback force increases with an increase in mass loading. Nasr and Ahmadi [48] have reported the effect of interparticle collision on turbulence modulation using the RANS k-ϵ model in a 2D vertical channel for $\mathrm{Re}_\tau \sim 644$. It was observed that fluid fluctuation decreases when interparticle collisions are considered. There is an increase in fluid fluctuation with an increase in volume loading if interparticle collisions are not considered. Wang *et al.* [49] have compared the results of the point particle method with the available experimental results. They have reported

that at low volume loading ($\phi_v \approx 3 \times 10^{-6}$), there is a good match between the simulation results with experiments, but at relatively higher volume loading, the simulations overpredicts near-wall concentration. Peng *et al.* [50] performed two-way coupled simulations for fully resolved neutrally buoyant particles using the lattice Boltzmann method (LBM). They considered the effect of particle rotation and lubrication effects between the particles in their study. They observed that the small particles have more tendency to form clusters compared to the larger ones. The clusters are found to be aligned along the streamwise direction. It is reported that the rate of production due to mean shear is reduced by the particles as velocity gradient is decreased in the buffer region. The regions of turbulence attenuation and augmentation were first classified based on the ratio of integral length scale and particle diameter [51]. Then, Tanaka and Eaton [52] found that there exists a region of attenuation between two augmentation regions depending upon the two dimensionless numbers based on particle Reynolds number and Stokes number.

Most of the studies which use LES models for the particle-laden flows are aimed to improve the prediction of particle statistics such as particle velocity, preferential concentration or segregation, etc., considering one-way coupling where turbulence modification is not considered. Soldati and Marchioli [53] investigated the sedimentation and resuspension in open channels, closed channels, and wavy channels at $\mathrm{Re}_\tau = 150$. They have used one-way coupling without any particle-particle interactions. The authors have commented about the need for particle subgrid scale models to accurately predict the particle concentration at low Stokes numbers. A summary of the literature on particle-laden LES for channel flow is given in Table I. There are only a few works reported on two-way coupled LES. Yamamoto *et al.* [1] considered two-way coupling and observed the turbulence attenuation for particles with small Stokes number. The important conclusion of their study was that the particle collisions are significant when volume fraction is even as small as order of 10^{-4}. Vreman *et al.* [10] and Mallouppas and van Wachem [5] studied the effect of two-way and four-way coupling in a vertical riser and horizontal channel cases, respectively. The effect of particles on turbulence modulation was found to be negligible as the considered volume fraction was very low in the study of Breuer and Alletto [13]. In a recent DNS study, Muramulla *et al.* [12] and Kumaran *et al.* [19] reported that turbulence attenuation increases as the volume fraction increase up to a certain volume loading, and then there is a drastic collapse in turbulence after which there is no change in turbulence intensities. In the present article, the volume loading at which the second moment of fluid velocity fluctuation decreases at least one order of magnitude compared to the unladen flow and the turbulence production collapses drastically has been referred to as critical particle volume loading (CPVL). The present paper covers two objectives: first, a detailed assessment of the performance in predicting the turbulence modulation for a range of volume fractions at the limit of high Stokes number; the other is to check the capability to predict critical volume loading at which there is a complete collapse of turbulence. To the best of our knowledge, the performance of the widely applied LES models, Smagorinsky, and dynamic Smagorinsky models to predict the turbulence modulation considering four-way coupled wall-bounded simulations for a wide range of volume fraction in the limit of high Stokes number has not been assessed so far.

The paper outline is as follows: In Sec. II, the methodology for LES and particle-phase equations is discussed along with simulation parameters. In Sec. III, fluid-phase statistics simulated with two subgrid scale (SGS) models are presented at two different Reynolds numbers. This is followed by the conclusions in the last section.

II. GOVERNING EQUATIONS

A. Fluid phase equations

The fluid phase has been considered to be incompressible and described by the filtered continuity and Navier-Stokes equations,

$$\frac{\partial \widetilde{u}_i}{\partial x_i} = 0 \qquad (1)$$

TABLE I. The Reynolds number, $Re_\tau = hu_\tau/2\nu$, particle Stokes number, $St = \rho_p d_p^2 \bar{u}/18\rho_f \nu h$, ϕ_{av} is the average volume fraction, $\bar{u}$ is the fluid bulk velocity, ρ_p and ρ_f are particle and fluid density, h is channel width, ν is kinematic viscosity, u_τ is the frictional velocity. Feedback force with an asterisk (*) includes the particle-particle collisions, $St^* = \rho_p d_p^2 u_\tau^2/18\rho_f \nu^2$.

	Reynolds number	Particle parameters	Mass loading and volume fraction	Feedback force
Wang and Squires (1996)	$Re_\tau = 180$	$St = 0.36-33$	$\phi_{av} = 3.4 \times 10^{-6}$ to 5.3×10^{-5}	One-way
	$Re_\tau = 644$	$St = 0.02-28$	$\phi_{av} = 2.3 \times 10^{-7}$ to 2.3×10^{-4}	
Wang and Squires (1996)	$Re_\tau = 180, 1000$	$St = 0.02-1.65$		One-way
Kuerten and Vreman (2005)	$Re_\tau = 180$	$St^* = 0.54-180$	$\phi_{av} = 6 \times 10^{-8}$	One-way
Kuerten (2006)	$Re_\tau = 150, 590$	$St^* = 1-25$		One-way
Marchioli et al. (2008)	$Re_\tau = 150$	$St = 0.047-1.18$	$\phi_{av} = 3.52 \times 10^{-5}$ to 4.4×10^{-3}	One-way
Marchioli et al. (2008)	$Re_\tau = 150$	$St = 0.00946-5.9$	$\phi_{av} = 3.12 \times 10^{-6}$ to 4.9×10^{-2}	One-way
Mazyar et al. (2010)	$Re_\tau \sim 350$	$St = 0.00013-2.25$	$\phi_{av} = 4.36 \times 10^{-11}$ to 9.6×10^{-5}	One-way
Vreman et al. (2009)	$Re_\tau = 180$	$St = 30.1$	$\phi_{av} = 1.3 \times 10^{-2}$	Two-way*
Breuer and Alletto (2012)	$Re_\tau \sim 350$	$St = 38.4$	$\phi_{av} = 7.3 \times 10^{-5}$	Two-way*
Mallouppas and Wachem (2013)	$Re_\tau = 600$	$St = 160$	$\phi_{av} = 4.79 \times 10^{-4}$	Two-way*
Yamamoto et al. (2001)	$Re_\tau = 644$	$St = 0.3-30$	$\phi_{av} = 0.17 \times 10^{-4}$ to 1.4×10^{-4}	Two-way*
Dritselis and Vlachos (2011)	$Re_\tau \sim 180$	$St^* = 25$ and 200	$\phi_{av} = 2.7 \times 10^{-5}$	Two-way*
Present study	$Re_\tau = 115$	$St = 105.47$	$\phi_{av} = 1 \times 10^{-4}$ to 2.8×10^{-3}	Two-way*
	$Re_\tau = 180$	$St = 179.74$		Two-way*

and

$$\frac{\partial \widetilde{u}_i}{\partial t} + \frac{\partial \widetilde{u}_i \widetilde{u}_j}{\partial x_j} = -\frac{1}{\rho_f}\frac{\partial \widetilde{p}}{\partial x_i} + \nu \frac{\partial^2 \widetilde{u}_i}{\partial x_j \partial x_j} + \frac{\partial (\widetilde{u}_i \widetilde{u}_j - \widetilde{u_i u_j})}{\partial x_j} + \frac{\widetilde{f}_i(x,t)}{\rho_f},\tag{2}$$

where $\widetilde{u}_i$ is the filtered velocity, $\widetilde{p}$ is the filtered pressure, ρ_f is the fluid density, and ν is the kinematic viscosity. $\widetilde{f}(x,t)$ is the feedback force by the suspended particles. Both the drag and lift forces are considered in the feedback force term and can be expressed as

$$\widetilde{f}_i(\mathbf{x},t) = -\sum_I \left(F_{i,I}^D + F_{i,I}^L\right)\delta(\mathbf{x} - \mathbf{x}_I),\tag{3}$$

where x_I is the position of the Ith particle, x is the fluid node, $F_{i,I}^D$ and $F_{i,I}^L$ are the drag and lift forces on the particle I, and $\delta(x - x_I)$ is the Dirac delta function in three dimensions. The third term on the right hand side of Eq. (2) is the subgrid scale stress and requires closure. We have used Smagorinsky and dynamic Smagorinsky formulations to model this term. Since the solid volume fraction is much lower compared to the continuum air volume fraction, we do not include any fluid volume fraction term ($\phi_v^{air} \approx 1$) in the fluid-phase momentum equation.

The in-house LES code "pLadenLES" is built upon an already validated direct numerical simulation (DNS) code [12]. The closure term in Smagorinsky and dynamic Smagorinsky models is calculated in physical space. The detailed simulation procedure for calculation of feedback force, near-wall corrections in lift and drag, and corrections for the undisturbed velocity at particle locations are discussed in an earlier work [12,19,20]. The LES code is verified by comparing the results with Ref. [12] for $\mathrm{Re}_b(\bar{u} \times 2\delta/\nu) = 3300$, where $\bar{u}$ is the bulk velocity and δ is half-channel width. The experimental data of Eckelmann [54] and DNS data from Muramulla *et al.* [12] and Moser *et al.* [55] are used to validate the $\mathrm{Re}_b = 5600$ case for unladen flow.

Smagorinsky and dynamic Smagorinsky model

Here, we briefly discuss the two widely applied Smagorinsky and dynamic Smagorinsky closure models used in the "pLadenLES" code. In the Smagorinsky model the SGS stress term ($\widetilde{u}_i \widetilde{u}_j - \widetilde{u_i u_j}$) is expressed as

$$-\tau_{ij} = \widetilde{u}_i \widetilde{u}_j - \widetilde{u_i u_j} = 2\nu_t \widetilde{S}_{ij},\tag{4}$$

$$\widetilde{S}_{ij} = \frac{1}{2}\left[\frac{\partial \widetilde{u}_i}{\partial x_j} + \frac{\partial \widetilde{u}_j}{\partial x_i}\right],\tag{5}$$

where ν_t is eddy viscosity, and $\widetilde{S}_{ij}$ is the filtered strain rate tensor. The eddy viscosity is written as

$$\nu_t = (C_s \widetilde{\Delta})^2 |\widetilde{S}|,\tag{6}$$

$$|\widetilde{S}| = \sqrt{2\widetilde{S}_{ij}\widetilde{S}_{ij}}.\tag{7}$$

In the above equation, $|\widetilde{S}|$ is the magnitude of the strain rate, C_s is the Smagorinsky coefficient, and $\widetilde{\Delta} = (\widetilde{\Delta}_1 \widetilde{\Delta}_2 \widetilde{\Delta}_3)^{1/3}$ is the cube-root volume of grid size. $\widetilde{\Delta}_1$, $\widetilde{\Delta}_2$, and $\widetilde{\Delta}_3$ are the grid spacing in the x, y, and z directions, respectively. $C_s = 0.125$ is used in the simulations. The specified C_s produces mean and second moments of the fluctuations which are comparable with the results of DNS for unladen flow. The van Driest damping is implemented to satisfy the wall-normal scaling of turbulent stress. A factor of $[1 - \exp(-y^+/A^+)]$ is multiplied with C_s, where y^+ is wall-normal distance in viscous units and $A^+ = 26$ [56]. In the case of the dynamic Smagorinsky model [57], the Smagorinsky coefficient is calculated dynamically with the time evolution of the velocity field rather than providing a constant value. Germano's identity is used to calculate the C_s and the tilde over tilde ($\widetilde{\widetilde{\cdot}}$) represents the second filtering operation over the filtered quantity. The Leonard stress (L_{ij}), grid-level stress, and test level stress tensor are related by Germano's identity to calculate the

Smagorinsky coefficient as follows:

$$L_{ij} = \widetilde{\widetilde{u_i}\widetilde{u}_j} - \widetilde{\widetilde{u}}_i\widetilde{\widetilde{u}}_j, \tag{8}$$

$$M_{ij} = 2\widetilde{\Delta}^2\widetilde{\widetilde{SS}}_{ij} - 2\widetilde{\widetilde{\Delta}}^2\widetilde{\widetilde{S}}\widetilde{\widetilde{S}}_{ij}, \tag{9}$$

$$C_s = \frac{\langle M_{ij}L_{ij}\rangle}{\langle M_{kl}M_{kl}\rangle}. \tag{10}$$

The box filter with twice the grid size is used as a test filter in the dynamic model to calculate the Smagorinsky coefficient (C_s). In this approach, two assumptions are made. First, the SGS stress scales with the filter width; i.e., C_s is a constant with the filter width, and second, C_s varies slowly in the space to be justifiable outside the integral. The averaging over the homogenous plane, which is expressed by ($\langle \ldots \rangle$), is required to avoid the negative value of C_s locally [58]. More details of the SGS models can be found elsewhere [57,58].

B. Particle phase description

The dynamics of discrete particles are described using Newton's second law of motion. Particle-particle and particle-wall interactions have been accounted for through the Lagrangian tracking of the particle center of mass. Particle-particle and particle-wall interactions are considered to be elastic and smooth. The particle motion is described by Eq. (11),

$$m_p\frac{dv_{i,I}}{dt} = F_{i,I}^D + F_{i,I}^L + \sum_{I\neq J}F_{i,IJ} + F_{i,Iw} + m_pg, \tag{11}$$

where $v_{i,I}$ is the velocity of the Ith particle, $F_{i,IJ}$ is the interaction force between the Ith and Jth particle, $F_{i,Iw}$ is the interaction force between the Ith particle and wall, g is the gravitational acceleration, $F_{i,I}^D$ is the drag force, and $F_{i,I}^L$ is the lift force exerted on the particle. The drag force is calculated using the inertia corrected drag law (Schiller-Naumann correlation [59]) as given here,

$$F_{i,I}^D = 3\pi\mu d_p[\widetilde{u}_{i,I}(x,t) - v_{i,I}]\left(1 + 0.15\text{Re}_p^{0.687}\right). \tag{12}$$

The collisions between the particle-particle and particle-wall have been modeled using hard-sphere elastic collisions. To calculate the drag, a point particle approximation has been used. However, in the near-wall region, the grid size in the wall-normal direction can be smaller than the particle size. Thus, the force on the grid is calculated from the fraction of particle surface present in the cell. Drag and lift have been calculated using the fluid interpolated velocity at the particle location. Detailed methods for interpolation of fluid velocity field and the correction due to self-perturbation induced by the particle have been reported in our earlier work [12].

C. Simulation methodology

The simulations have been performed in a vertical channel with dimensions $8\pi\delta \times 2\delta \times (4/3)\pi\delta$ in streamwise (x), wall-normal (y), and spanwise (z) directions, respectively (Fig. 1), where δ is the half-channel width. The pseudospectral method is used for solving filtered Navier-Stokes equations. No-slip boundary conditions are applied on the walls. The Smagorinsky and dynamic Smagorinsky models are used for subgrid scale (SGS) closure. Simulations are performed at two bulk Reynolds numbers ($\text{Re}_b = \rho_f \times \bar{u} \times 2\delta/\mu_f$) 3300 and 5600 based on the channel width (2δ) and average fluid velocity ($\bar{u}$). The Reynolds number based on the unladen frictional velocity and half-channel width, Re_τ, corresponds to 115 and 180, respectively. In our simulations, flow is resolved with $64 \times 65 \times 32$ and $128 \times 65 \times 64$ grid points for bulk Reynolds numbers of 3300 and 5600, respectively. For Reynolds number of 5600, the grid resolution is decided as per the study of Wang and Squires [36]. The number of grids for lower Reynolds number ($\text{Re}_b = 3300$) is decreased in order to have almost the same Δx^+ and Δz^+ as for $\text{Re}_b = 5600$. In the present study, $\Delta x^+ = 45$, $\Delta z^+ = 15$ and
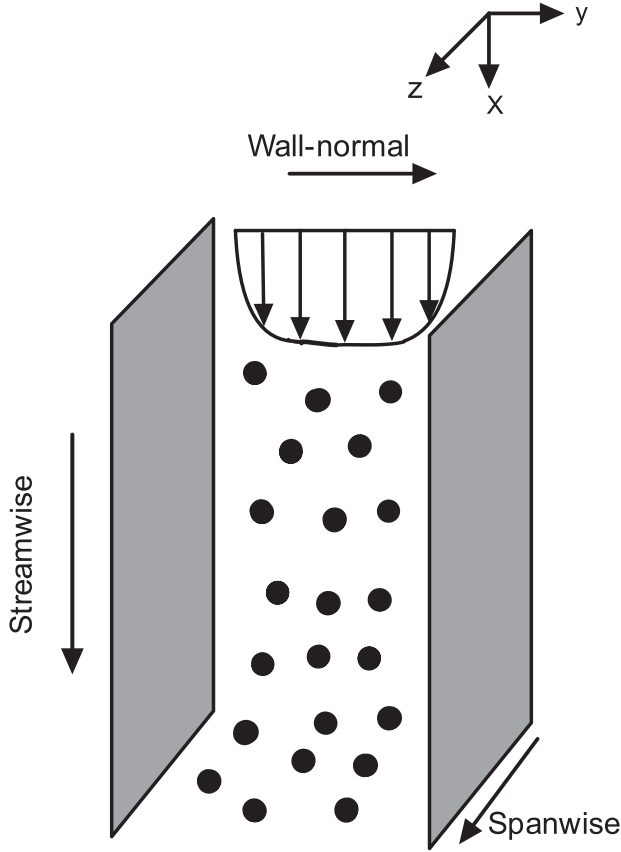
FIG. 1. Schematic of the vertical channel.

$\Delta x^+ = 35$, $\Delta z^+ = 12$ are used for Reynolds number of 3300 and 5600, respectively. The number of grids used for the computations is the same for both the LES models. The first grid point in the wall-normal direction is such that y^+ is less than 1. The ($^+$) symbol indicates that the quantity is normalized with viscous scales. The time step used in the simulations is ($0.0083h/\overline{u}$), where $h = (2\delta)$ is channel width and $\overline{u}$ is fluid bulk velocity. The pressure gradient is adjusted to maintain a constant bulk flow rate. We have validated the LES results for unladen flows and provided the results in the Appendix. The results on two-phase velocity statistics for both the Reynolds number of 3300 and 5600 are compared with DNS results [12].

The material density of the particle (ρ_p) is 2000 kg/m^3 and the diameter (d_p) is 39 μm. As the density ratio of the particle to fluid is higher, the buoyancy and Basset history effects are neglected in the particle's equation of motion. The Stokes number (St $= \tau_p/\tau_f$) is 105.47 and 179.74 for Reynolds number of 3300 and 5600, respectively. Here, the viscous relaxation time of the particle is $\tau_p = \rho_p d_p^2/18\mu_f$ and the fluid time scale is $\tau_f = 2\delta/\overline{u}$. Few of the earlier studies [1,30,31,33] considered the fluid time scale based on the viscous units. The main focus of those investigations was to perform LES to predict the particle dynamics and concentration profiles in particle-laden flows. Those studies were performed using the one-way coupled technique for low volume fractions. Therefore, variation of the friction velocity and a consequent change in computed fluid time scale were not captured. On the other hand, Kulick *et al.* [7], Vreman *et al.* [10], and Gualtieri *et al.* [60] used the Kolmogorov time scale to obtain the Stokes number. Their studies were motivated toward the prediction of preferential clustering of the particles. To address the large scale fluctuating dynamics in particle laden flows, Vreman [14], Kumaran *et al.* [19], Squires and Eaton [3], and
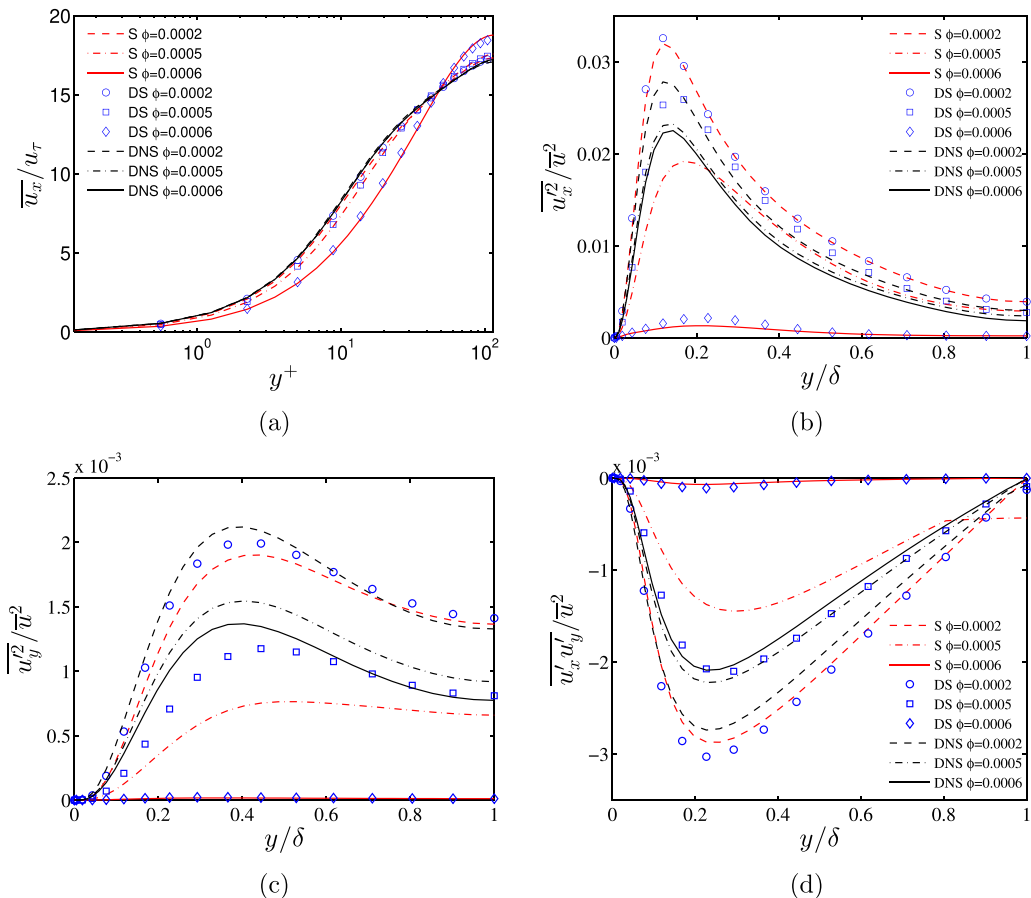
FIG. 2. Fluid phase velocity statistics. (a) Streamwise mean velocity normalized by unladen frictional velocity. (b) Streamwise fluid fluctuations. (c) Wall-normal fluctuations. (d) Cross-stream stress normalized by bulk velocity. S: Smagorinsky model. DS: Dynamic Smagorinsky model. DNS: Direct numerical simulation. Bulk-averaged Reynolds number (Re_b) is 3300.

Muramulla *et al.* [12] have used the integral scale to obtain the particle Stokes number. In the present study, the simulations are performed at high volume fractions using the two-way coupled technique. A significant change in the frictional velocity with an increase in particle loading is observed [as shown in Fig. 2(a)]. This leads to a variation in the fluid time scale computed using friction velocity if particle volume fraction is increased. Therefore, the fluid time scale in the viscous unit is a simulation output. It is worth mentioning that the bulk averaged fluid velocity is the same for all the particle volume fractions. The present article deals with the modulation of turbulent intensities and modification of turbulence production, which are related to large scale fluctuations. Therefore, we have chosen an integral fluid time scale ($\delta/\bar{u}$), which is the same for all the particle loading and can be calculated using input variables. The Stokes numbers based on the viscous scale (for unladen cases) are 1718.1 and 4231.8, which correspond to the Stokes numbers 105.47 and 179.74, calculated using the integral fluid time scale.

III. RESULTS

First, we discuss turbulence modulation and collapse with the increase in particle volume fraction. The predictions by LES models are compared with the DNS results. Then we explore

the origin of the differences in results predicted by LES compared to DNS through the analysis of fluid-particle relative velocity distributions, momentum, and energy balances of fluid phase at different particle loading. In all the figures, plots in red lines are shown for Smagorinsky, blue colored lines are for dynamic Smagorinsky, and the black lines are for DNS and filtered DNS. The notations S in the legends are used for Smagorinsky, DS for dynamic Smagorinsky, DNS for direct numerical simulation, and FDNS for filtered DNS throughout the article.

A. Fluid phase velocity statistics

Fluid phase statistics obtained from LES of the particle-laden flows are compared with DNS for Reynolds number of 3300 as shown in Fig. 2. In Fig. 2(a), streamwise mean velocity normalized by unladen frictional velocity is plotted as a function of wall-normal distance for a wide range of solid volume fractions. For both the LES models, the mean velocity starts to deviate from the DNS profile as the volume fraction (ϕ) increases beyond 2×10^{-4}. Both the models show a decrease in velocity at the viscous sublayer and buffer layer, but at the channel center, the velocity is higher than that predicted by DNS. This happens up to a volume fraction of 6×10^{-4} in LES for both the models. The departure from the DNS results becomes more prominent at a volume fraction of 6×10^{-4}, which is related to the overprediction of turbulence modulation by LES models at that volume fraction. Figures 2(b)–2(d) show the second moments of the fluid velocity fluctuations normalized by the average fluid velocity. The streamwise fluid fluctuations are overpredicted compared to DNS at low volume fractions. The fluid fluctuations decrease as the volume fraction is increased. For streamwise mean square fluctuations, there is only 22% decrease in the peak value as the volume fraction is increased from 0 to 6×10^{-4} for DNS. However, there is a prediction of 50% and 30% decrease in the peak value for streamwise fluid fluctuations as the volume fraction is increased from 0 to 5×10^{-4} for the Smagorinsky and dynamic Smagorinsky model, respectively. Then, a further increase in volume fraction from 5×10^{-4} to 6×10^{-4} results in an almost 1.5 order of magnitude decrease for both the LES models. A similar observation on the decrease in the streamwise fluid fluctuations was reported by Muramulla *et al.* [12] at a higher volume fraction (10^{-3}) using DNS study.

A drastic decrease is also observed in the second moment of wall-normal fluctuation. There is a 45% decrease in the peak value of $u_y'^2/\overline{u}^2$ as volume fraction is increased from 0 to 6×10^{-4} in the DNS predictions. However, there is 70% and 60% decrease in the wall-normal fluid fluctuations as the volume fraction is increased from 0 to 5×10^{-4} for the Smagorinsky and dynamic Smagorinsky model, respectively. A further increase in volume fraction from 5×10^{-4} to 6×10^{-4} results in almost two orders of magnitude decrease for both the LES models. There is 60% and 40% decrease in the Reynolds stress as the volume fraction is increased from 0 to 5×10^{-4} for the Smagorinsky and dynamic Smagorinsky model, respectively. However, only a 30% decrease in Reynolds stress is predicted by DNS for an equivalent increase in the particle volume loading as shown in Fig. 2(d). If the volume fraction is increased from 5×10^{-4} to 6×10^{-4}, there is prediction of almost 1.5 orders of magnitude decrease in Reynolds stress by both the LES models. For the same St and Re_b, the decrease of approximately 1.5 orders of magnitude in the Reynolds stress was reported in Ref. [12] from the DNS study if ϕ is increased to 1×10^{-3}. A similar exercise is performed at a moderate Reynolds number ($\mathrm{Re}_b = 5600$). The results show a similar feature of a drastic decrease in turbulence intensity beyond a certain volume fraction and overprediction of turbulence attenuation by LES models compared to DNS. The figures to show the variation of different components of fluctuations are not shown here, but a channel averaged description is provided below.

The above discussion demonstrates that both the LES models successfully predict turbulence attenuation with increased particle volume fraction. However, at a relatively higher volume fraction, the extent of turbulence attenuation is overpredicted by the LES models compared to DNS. Since the modulation of turbulence fluctuations is not the same at all the wall-normal locations, a wall-normal averaged value for different volume fractions can be a good indicator to quantify the extent of turbulence modulation. Such a method may also help to identify the volume fraction at which
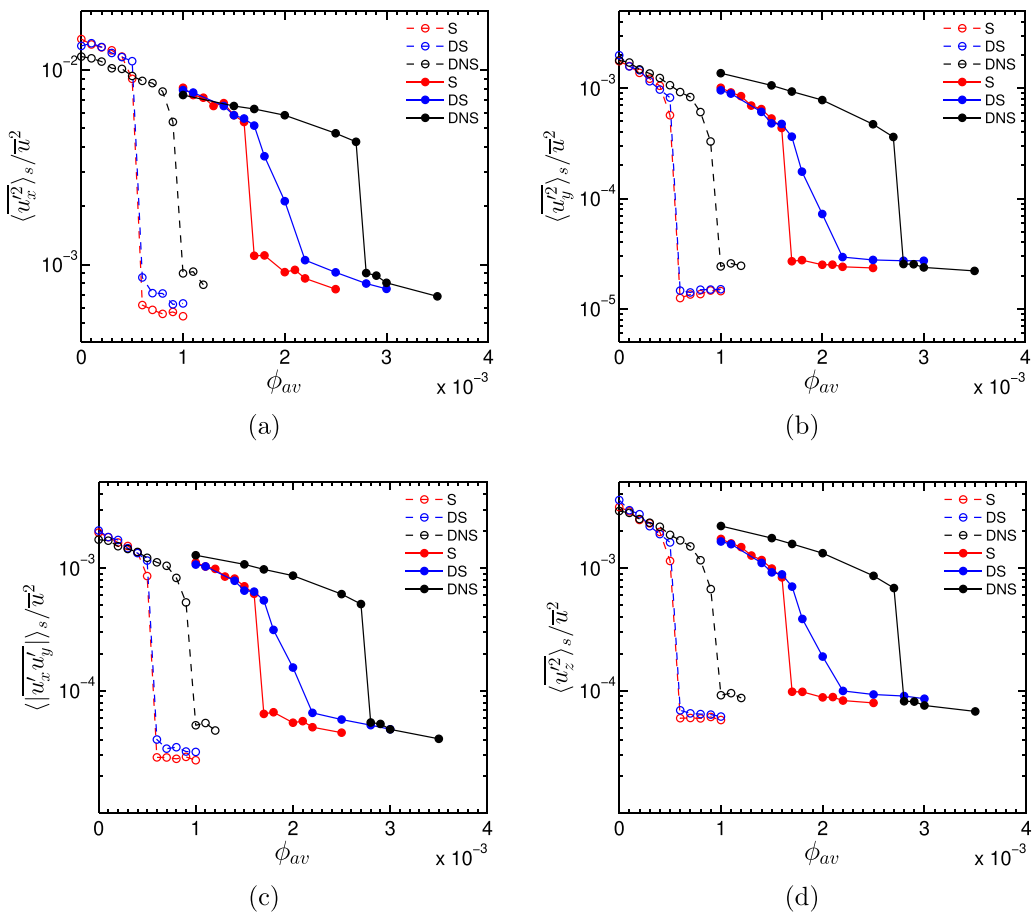
FIG. 3. Average of second moments of fluid velocity fluctuations plotted for a range over average volume fractions (ϕ_{av}). (a) Streamwise, (b) wall-normal, (c) cross-stream, and (d) spanwise direction. The dashed lines with open symbols are for $\mathrm{Re}_b = 3300$, and solid lines with filled symbols are for $\mathrm{Re}_b = 5600$. S: Smagorinsky model. DS: Dynamic Smagorinsky model. DNS: Direct numerical simulation.

turbulence collapses drastically. Hereafter, this article will refer to this volume fraction as the critical particle volume loading (CPVL).

B. Modulation of turbulent intensity

In this section, we focus on exploring the capability of LES models more precisely. We compute the average turbulent fluctuations across the channel as a function of particle volume loading and pinpoint the CPVL at which turbulence collapses. In Fig. 3, it is shown that initially, with an increase in solid volume fraction, all the components of turbulent velocity fluctuation decrease monotonically to 60% (or higher) of unladen fluid velocity fluctuations. Then, there is a drastic decrease in turbulence fluctuation at a particular volume loading, which is at least one order of magnitude lower than the unladen flow. The extent of decay may be higher depending on the component of fluid fluctuation being considered and the fluid phase Reynolds number. The specific volume loading at which such a discontinuous decrease is observed has been referred as critical particle volume loading (CPVL). It is worth mentioning that the CPVL depends on the Stokes number and fluid phase Reynolds number [12]. The present methodology of computing average fluctuations across

the channel helps us identify the differences in turbulence intensity predicted by LES compared to DNS for a wide range of volume fractions and helps to determine the extent of underprediction in CPVL. The averaged fluid fluctuations are calculated using Eq. (13) and are plotted in Fig. 3. The fluctuations are normalized by the square of bulk velocity,

$$\langle \star \rangle_s = \frac{1}{\delta} \int_0^\delta dy \langle \star \rangle. \tag{13}$$

It is observed that all the second moments of fluctuations decrease with an increase in volume loading, and then there is a sudden collapse of fluctuations at CPVL. Figure 3 shows that for $Re_b = 3300$, the CPVL as predicted by DNS is 10^{-3} (CPVL$_{DNS}$). The Smagorinsky and dynamic Smagorinsky models predict turbulence collapse at $\phi = 0.0006$ (CPVL$_{LES}$), which is much lower than that predicted by DNS. For both the LES models, the streamwise fluctuations are overpredicted compared to DNS before the turbulence collapse ($\phi = 6 \times 10^{-4}$) [Fig. 3(a)]. However, the wall-normal fluctuations, spanwise fluctuations, and the Reynolds stress match well with the DNS results for low volume fractions, and start deviating near critical loading predicted by both the LES models [see Figs. 3(b)–3(d)]. For a particle loading less than 6×10^{-4}, the maximum deviation for the model prediction is found to be 20% of the DNS results.

In Fig. 3, it is shown that for bulk Reynolds number of 5600, the critical loading predicted by the DNS, Smagorinsky, and dynamic Smagorinsky models are 2.8×10^{-3}, 1.7×10^{-3}, and 2.2×10^{-3}, respectively. Therefore, it is evident that the dynamic Smagorinsky model performs better to predict the critical volume loading at a moderate Reynolds number. The underprediction of the CPVL by the Smagorinsky model may originate due to the higher subgrid scale dissipation compared to the dynamic Smagorinsky model, which is discussed a little later.

Figures 4(a)–4(d) show a marginal overprediction of all the fluctuating velocities at low volume fraction, which decreases with an increase in volume loading till the CPVL$_{LES}$ is reached. A maximum deviation of 20% in the model prediction is observed in the second moments of velocity fluctuations by the dynamic Smagorinsky model as shown in Fig. 4. Figure 5 shows the ratio of the LES predictions compared to DNS at Reynolds number of 5600. It is observed from Fig. 5 that the second moments of fluid velocity fluctuations in streamwise, spanwise, and Reynolds stress component predicted by LES models deviate by a maximum of 20% at a volume loading of 10^{-3} from the DNS prediction. However, in the wall-normal direction, it is about 30%. The deviation in LES predictions increases as the CPVL$_{LES}$ is approached, which may be due to an increase in subgrid scale modeling error at higher volume fractions, which will be further discussed in Sec. III E. It is worth noting that the LES simulations predict the second moments with reasonable accuracy up to a higher volume loading when the Reynolds number is increased. It is observed from the prediction of the second moments of turbulent velocity fluctuations that both the Smagorinsky and dynamic Smagorinsky models perform equivalently, and underpredict the critical volume loading compared to DNS at low Reynolds number ($Re_b = 3300$). However, at moderate Reynolds number ($Re_b = 5600$), prediction by dynamic Smagorinsky is better than the Smagorinsky model (Fig. 5). To understand whether subgrid scale dissipation plays any role, we have computed the time average C_s values for the dynamic Smagorinsky model for different volume loading and compared with the C_s value for the Smagorinsky model, including the van Driest damping function. We observe that at lower Reynolds number, the values compare well till the critical volume loading (CPVL$_{LES}$), but at Reynolds number ($Re_b = 5600$), the average C_s decreases for the dynamic model when it approaches the volume fraction of 1.5×10^{-3}, which is lower than the C_s value used in the Smagorinsky model. Consequently, the dynamic model shows collapse at marginally higher volume loading compared to the Smagorinsky model (Fig. 6).

Another important observation in the above results is the underprediction of the CPVL by LES models compared to DNS, albeit there is no difference in the mean particle concentration profile as predicted by LES compared to DNS (figures are not shown here). We have performed the following investigations to understand the reason for the deviation of second moments predicted by LES
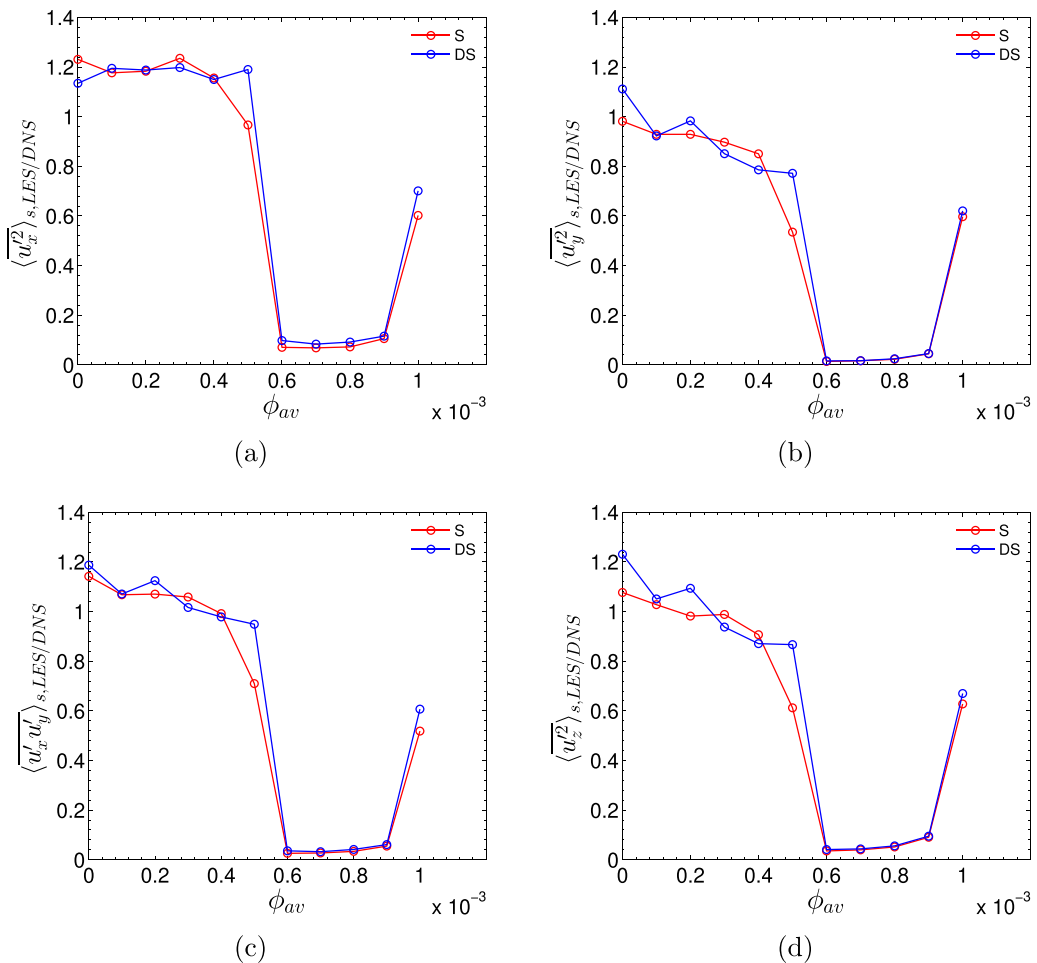
FIG. 4. The ratio of the second moments of the velocity fluctuations with respect to DNS as a function of average volume fractions (ϕ_{av}) for $\mathrm{Re}_b = 3300$. (a) Streamwise, (b) wall-normal, (c) cross-stream, and (d) spanwise direction. S: Smagorinsky model. DS: Dynamic Smagorinsky model.

models at higher volume fraction, and their failure to predict the critical volume loading. First, we check whether there is any significant deviation in the LES prediction for fluid-particle relative velocity distribution and a consequent difference in the calculated interphase momentum transfer. Next, we have computed all the terms of the mean momentum equation, and energy equations of mean flow and fluctuating fields. In all the cases, results are compared with the DNS. To quantify the effect of filtering, in an earlier study Marchioli *et al.* [33] have performed an *a priori* study by filtering the DNS fluid field and calculating the particle phase statistics. Those statistics were compared with the prediction of DNS. Such a study quantifies the error induced by the filtering. It is to be noted that the authors performed the simulations using one-way coupling. However, the present investigation is performed using two-way coupling between the fluid and particle phases. Therefore, we need to modify the testing scheme to establish the effect of filtering. The filtered fluid field is calculated from the DNS study, and using that filtered field, we calculate the relative velocity of fluid and particle phase, and compute their distribution function. In this DNS study, the filtered data are used only to calculate the relative velocity; we do not use the filtered field in the particle equation of motion and subsequent calculation of feedback force to the fluid phase. Following this method, we
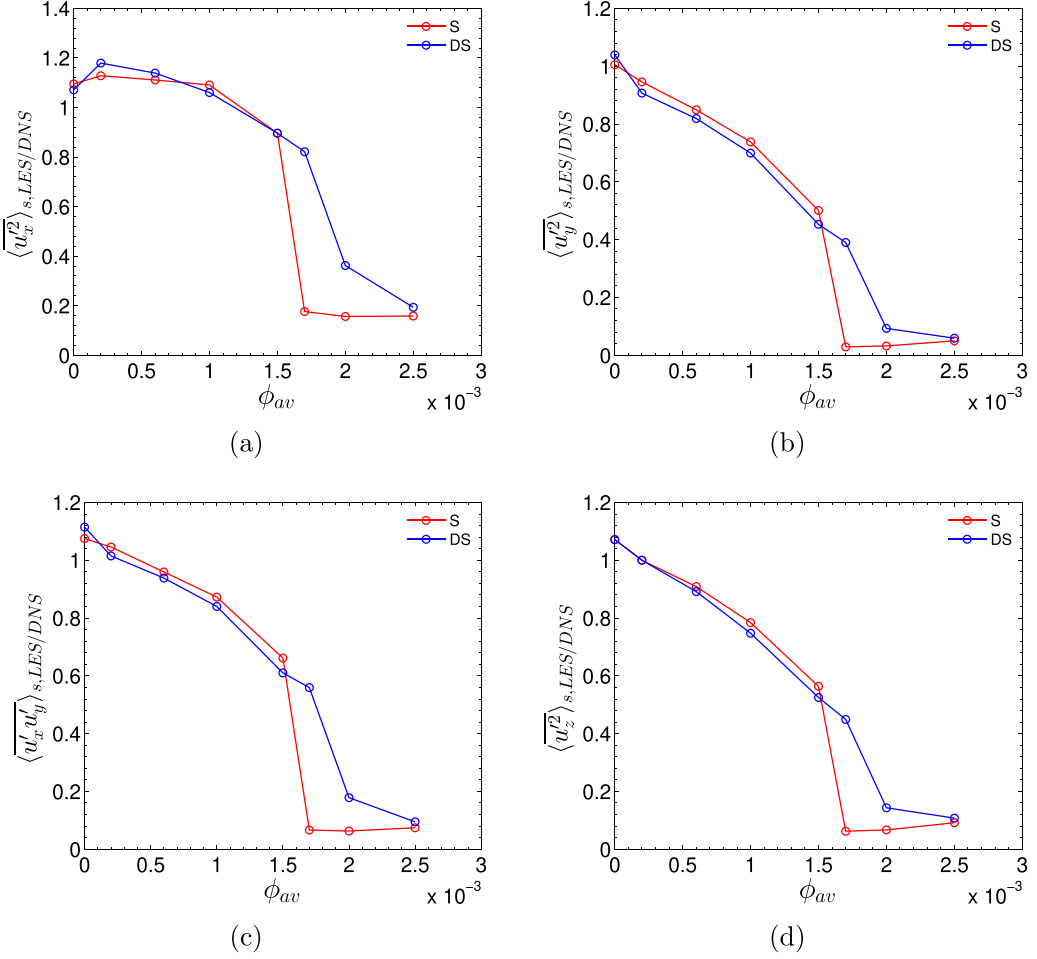
FIG. 5. The ratio of second moments of the velocity fluctuations with respect to DNS as a function of average volume fractions (ϕ_{av}) for $Re_b = 5600$. (a) Streamwise, (b) wall-normal, (c) cross-stream, and (d) spanwise direction. S: Smagorinsky model. DS: Dynamic Smagorinsky model.

avoid data corruption of DNS by the effect of filtering during time marching. To quantify the filtering error in predicting the relative velocity, filtered DNS is performed for both the Reynolds number. The cutoff filter with twice the grid size is implemented in homogenous directions to calculate the filtered velocity.

C. Relative velocity statistics

In this section, we discuss the probability density function of the streamwise component of the relative velocity. We also report the average relative velocity between the particle and fluid phases. The normalized distribution functions are computed at two zones inside the channel; one is at the channel center ($y/\delta = 0.9$–1.1) and the other one is near the wall ($y/\delta = 1.85$–1.95). Figures 7(a)–7(d) show the results for two solid volume fractions of $\phi = 5 \times 10^{-4}$ and $\phi = 6 \times 10^{-4}$ at $Re_b = 3300$. The first one is lower than the CPVL shown by the LES models (CPVL$_{LES}$, $\phi = 6 \times 10^{-4}$). It is observed in Figs. 7(a) and 7(c) that the shape of the distribution functions computed from the LES models are very similar to that predicted by DNS at both the locations at
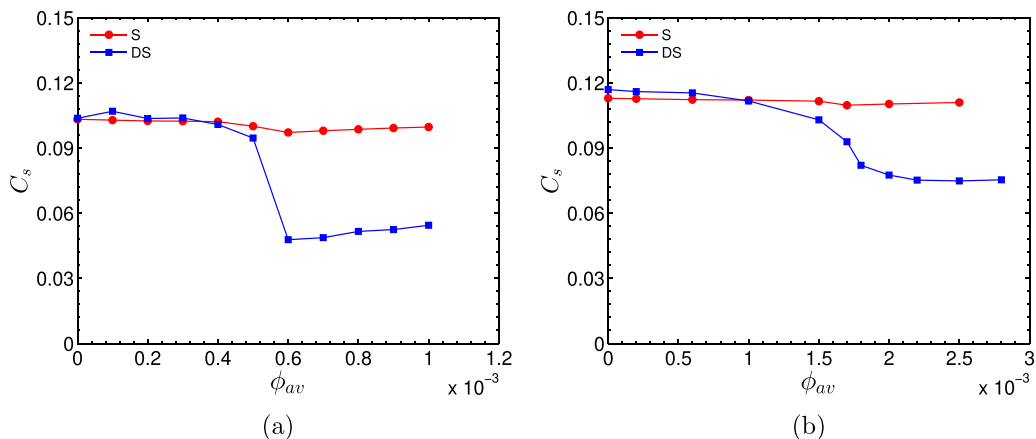
FIG. 6. The Smagorinsky coefficient averaged across the channel width for different volume fractions (ϕ_{av}) for (a) $Re_b = 3300$, (b) $Re_b = 5600$. S: Smagorinsky model. DS: Dynamic Smagorinsky model.

a volume fraction lower than the $CPVL_{LES}$. There is only a minor difference in the variance of the fluctuations at the center of the channel. At higher volume loading ($\phi = 6 \times 10^{-4}$), the pattern of the model predicted distribution function varies significantly as shown in Figs. 7(b) and 7(d). This is because, at the volume fraction of 6×10^{-4}, both the LES models show a turbulence collapse, but DNS does not. Gaussian plots corresponding to the DNS results depict that distributions are Gaussian up to more than two decades in all the figures. The relative velocity distribution functions at moderate Reynolds number ($Re_b = 5600$) are presented in Fig. 8. It is observed that the patterns of the model predicted distribution functions are similar to the DNS, even though there is a significant difference in the mean and the variance of the relative velocity distribution. The difference in distribution for filtered DNS (FDNS) compared to DNS is observed only in the near-wall region at low Reynolds number ($Re_b = 3300$) as shown in Figs. 7(c) and 7(d). However, at $Re_b = 5600$, the differences exist at both the channel center and near-wall locations as shown in Fig. 8. Besides the distribution function, calculation of the first moment of the distribution function, i.e., the mean relative velocity, provides information about the accuracy of the LES models to predict average drag force exerted on the fluid phase.

Mean relative velocities (slip velocity) as a function of particle volume fraction are shown in Figs. 9(a) and 9(b) for Reynolds numbers of 3300 and 5600, respectively. It is shown that the particle leads the air near the wall region but lags at the center of the channel. Relative velocity near the wall increases slowly with the increase in volume fraction up to 5×10^{-4} for $Re_b = 3300$ [Fig. 9(a)]. After that, there is almost 50% increase in relative velocity as predicted by the models. However, DNS data show a monotonic increase at that point. In the case of a moderate Reynolds number ($Re_b = 5600$), both the models and DNS do not show any significant variation of relative velocity. However, the Smagorinsky model predicts a sharp increase of relative velocity (at $CPVL_{LES}$ predicted by the same model) at the "near-wall" region. At this volume fraction, the dynamic Smagorinsky model shows a gradual increase in relative velocity. A percentage difference of relative velocity predicted by the models in comparison to the DNS is shown in Figs. 9(c) and 9(d). A difference as low as 3% is shown at a volume fraction of 10^{-4}. It increases monotonically with volume fraction up to the critical volume fraction (predicted by LES). After that, there is a sharp change when the turbulence collapses. A similar variation is also observed in the drag term in momentum balance for mean flow, which is discussed in the next section. The simulations performed using filtered DNS show that the filtering effect contributes a maximum of 6% and 15% differences in the average relative velocity when compared to DNS for Reynolds number of 3300 and 5600, respectively. The filtering effect is larger in the near-wall region than the channel center,
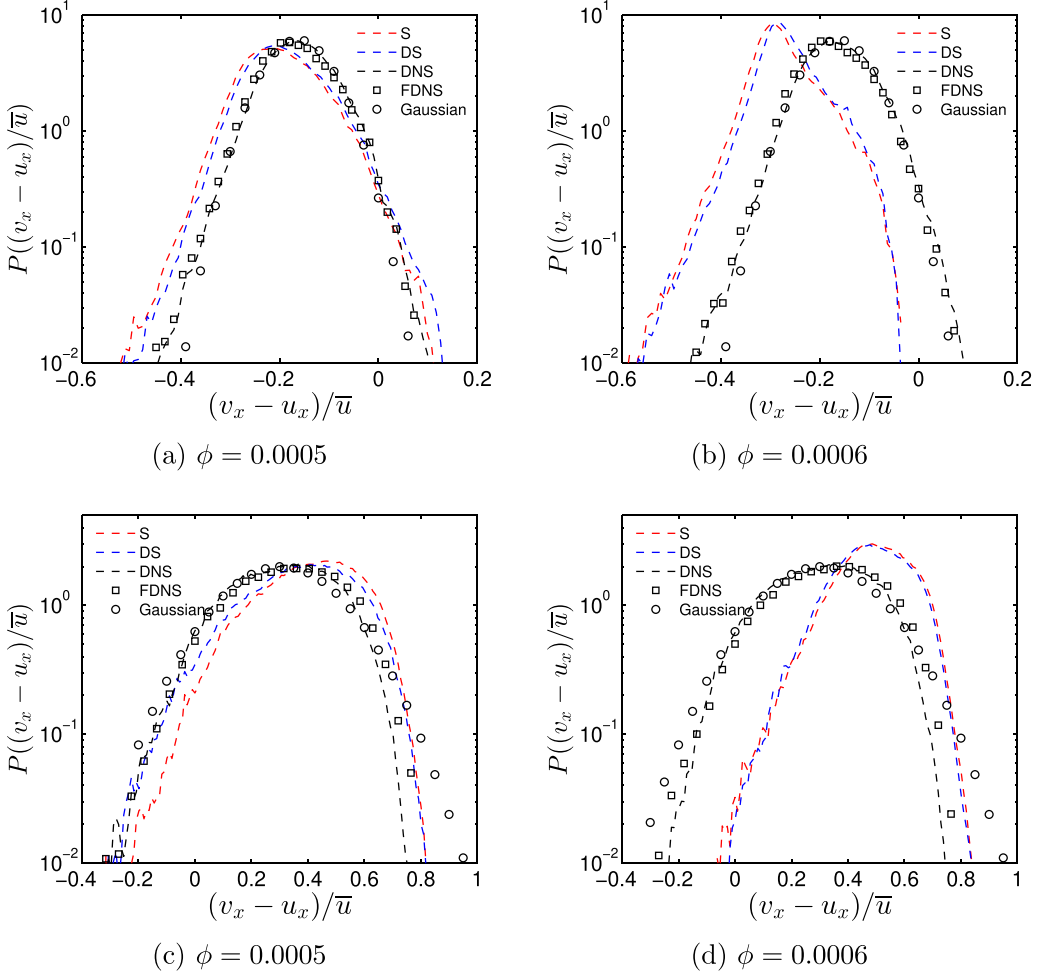
FIG. 7. Relative velocity distribution for $\mathrm{Re}_b = 3300$. Panels (a) and (b) are plotted for the channel center location where $y/\delta = 0.9\text{--}1.1$. Panels (c) and (d) are plotted for near-wall region where $y/\delta = 1.85\text{--}1.95$. S: Smagorinsky model. DS: Dynamic Smagorinsky model. DNS: Direct numerical simulation. FDNS: Filtered DNS.

and does not change significantly with the particle volume loading except very near the critical volume loading. Such an observation is an indication that the modeling error may contribute more than the filtering error toward the deviation of relative velocity from the DNS measurement. In this context, it is worth mentioning that in an earlier study by Boivin *et al.* [4], it was reported that modeling error has less effect for the particle-laden flows compared to the unladen flows in the limit of high mass loading. It is to be noted that the authors performed the simulations for homogeneous isotropic turbulence at a particle volume fraction of $O(10^{-4})$. Therefore, the effect of anisotropy and the role of subgrid scales did not introduce any error in their simulations when there is a suppression of the overall turbulence production. On the other hand, Dritselis and Vlachos [61] have commented that, for the particle-laden channel flow, modeling error has a higher impact in the limit of high Stokes number. To understand the source of the deviation in LES prediction compared to DNS, we have computed the different terms of the momentum and energy balance equations, and compared with the DNS results in the following sections.
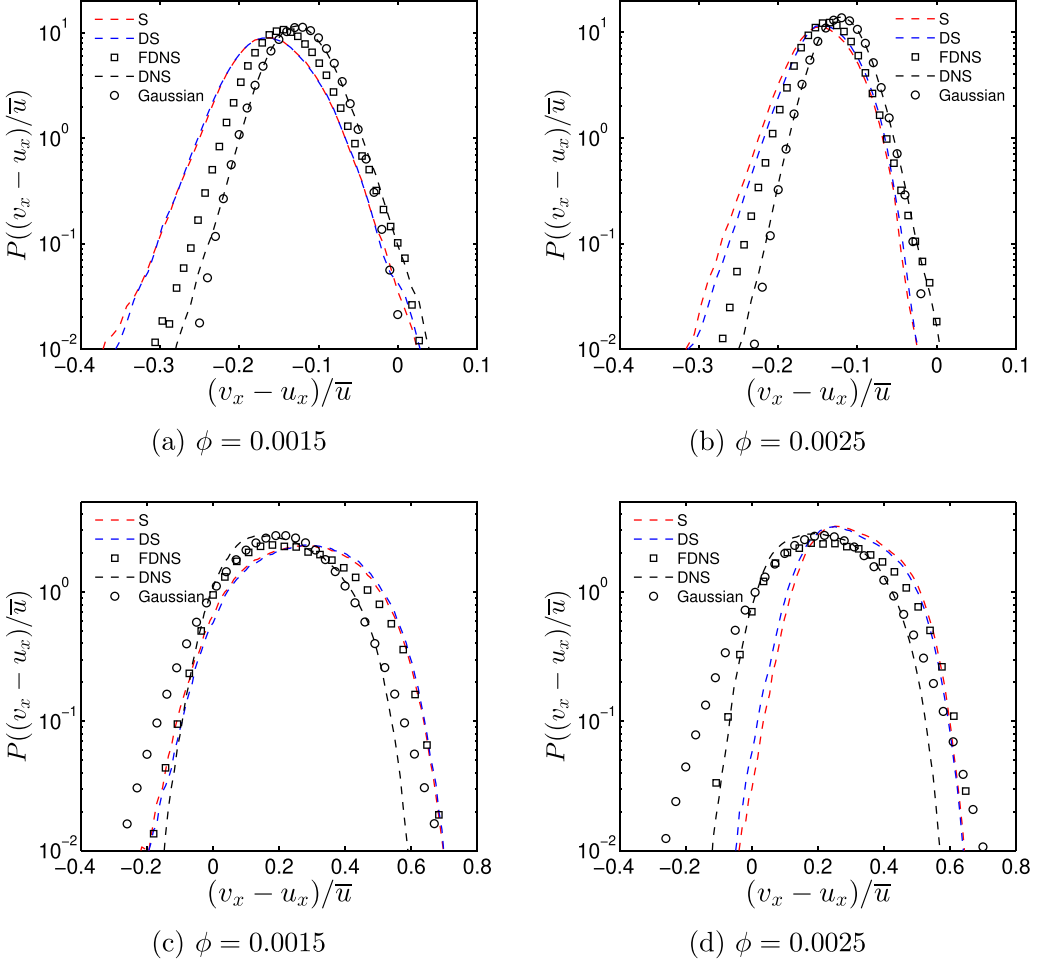
FIG. 8. Relative velocity distribution for $\mathrm{Re}_b = 5600$. Panels (a) and (b) are plotted for the channel center location where $y/\delta = 0.9$–1.1. Panels (c) and (d) are plotted for near-wall region where $y/\delta = 1.85$–1.95. S: Smagorinsky model. DS: Dynamic Smagorinsky model. DNS: Direct numerical simulation. FDNS: Filtered DNS.

D. Fluid phase momentum balance

The streamwise and wall-normal components of filtered momentum equations are presented as

$$-\frac{1}{\rho_f}\frac{\partial \widetilde{P}}{\partial x} - \frac{\partial(\overline{\widetilde{u'_x}\widetilde{u'_y}})}{\partial y} + (\nu + \nu_t)\frac{\partial^2(\widetilde{U}_x)}{\partial y\partial y} - \overline{\frac{\rho_p f\phi_c}{\rho_f \tau_p}(\widetilde{u}_x - \widetilde{v}_x)} = 0 \tag{14}$$

and

$$-\frac{1}{\rho_f}\frac{\partial \widetilde{P}}{\partial y} - \frac{\partial(\overline{\widetilde{u'_y}\widetilde{u'_y}})}{\partial y} - \overline{\frac{\rho_p f\phi_c}{\rho_f \tau_p}(\widetilde{u}_y - \widetilde{v}_y)} = 0. \tag{15}$$

Here, $\overline{\widetilde{p}} = \widetilde{P}$; $\widetilde{p}$ is the instantaneous filtered pressure and $\widetilde{P}$ is the mean filtered pressure. Similarly, $\widetilde{u}$ is the instantaneous filtered velocity, $\widetilde{U}_x$ is the mean filtered velocity, and $\widetilde{u}'$ is the filtered fluctuating velocity. $\rho_f \overline{\widetilde{u'_i}\widetilde{u'_j}}$ is filtered Reynold stress (τ^R_{ij}), ϕ_c is the volume fraction in respective grid, f is the
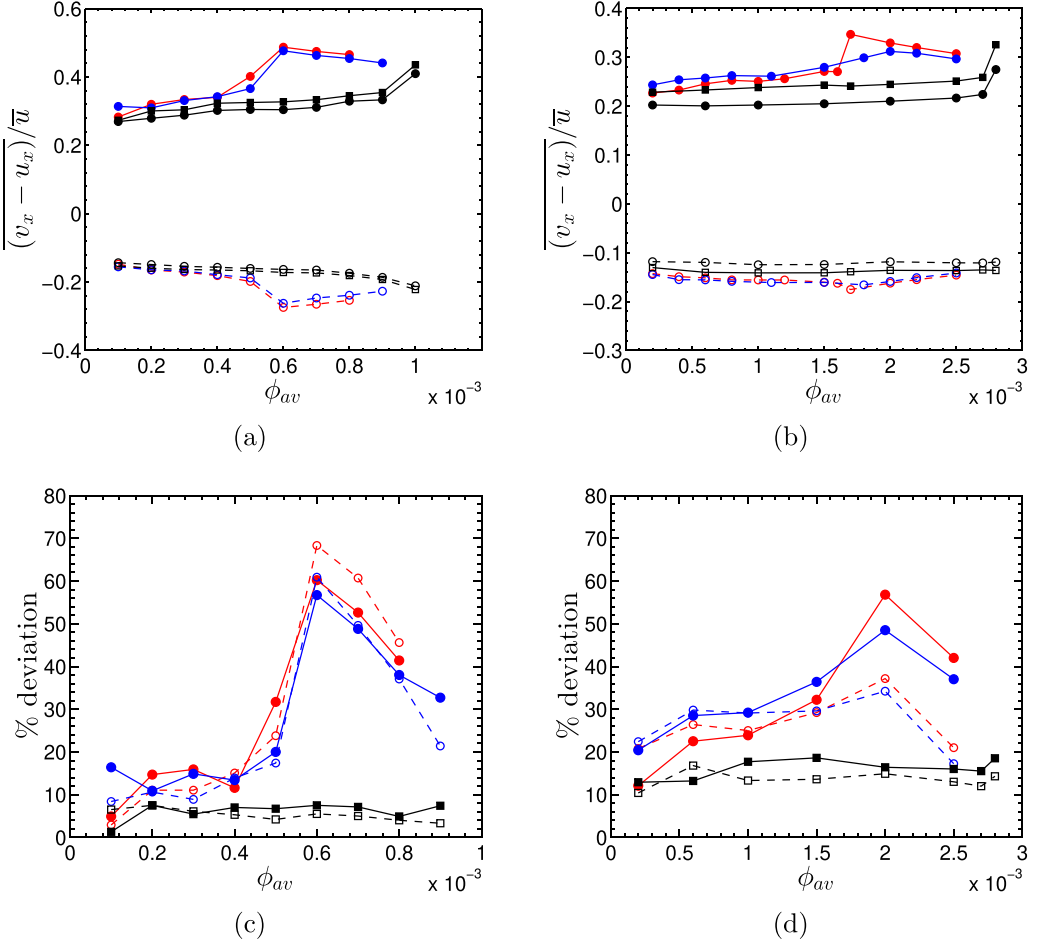
FIG. 9. Mean relative velocity as a function of average volume fraction at (a) $Re_b = 3300$, (b) $Re_b = 5600$. Deviation of mean of relative velocity with respect to DNS at (c) $Re_b = 3300$, (d) $Re_b = 5600$. Near-wall region is shown with solid lines and channel center zone is shown with dashed line. S: Smagorinsky model (red lines). DS: Dynamic Smagorinsky model (blue lines). DNS: Direct numerical simulation (black lines with circles). FDNS: Filtered direct numerical simulation (black lines with square symbols).

drag coefficient, τ_p is the particle relaxation time, and the last terms in Eqs. (14), and (15) are the feedback forces in streamwise and wall-normal directions, respectively.

The terms which appear in the momentum balance equation (14) are plotted in Fig. 10 along with the wall-normal distance. All the terms are scaled with $\bar{u}^2/2\delta$. Figure 10 presents the effect of volume fraction at bulk Reynolds number of 3300 on different terms appearing in the momentum balance equation. It is shown in Fig. 10(a) that at a low volume fraction of 3×10^{-4} all the terms match well with the DNS predicted values. Divergence of viscous stress and Reynolds stress are found to be comparable in magnitude. With increasing particle volume loading, a significant variation in the divergence of Reynolds stress is observed, and it essentially collapses at a volume fraction of 6×10^{-4}, which is a critical volume fraction predicted by LES. The model predicted values of divergence of stress terms start to deviate significantly from the DNS predicted values as we approach the CPVL$_{LES}$. At critical volume loading, the pressure gradient is balanced with the divergence of viscous stress and the drag force exerted by the particles. In this context, we also report the accuracy of models to predict the divergence of viscous stress at different volume
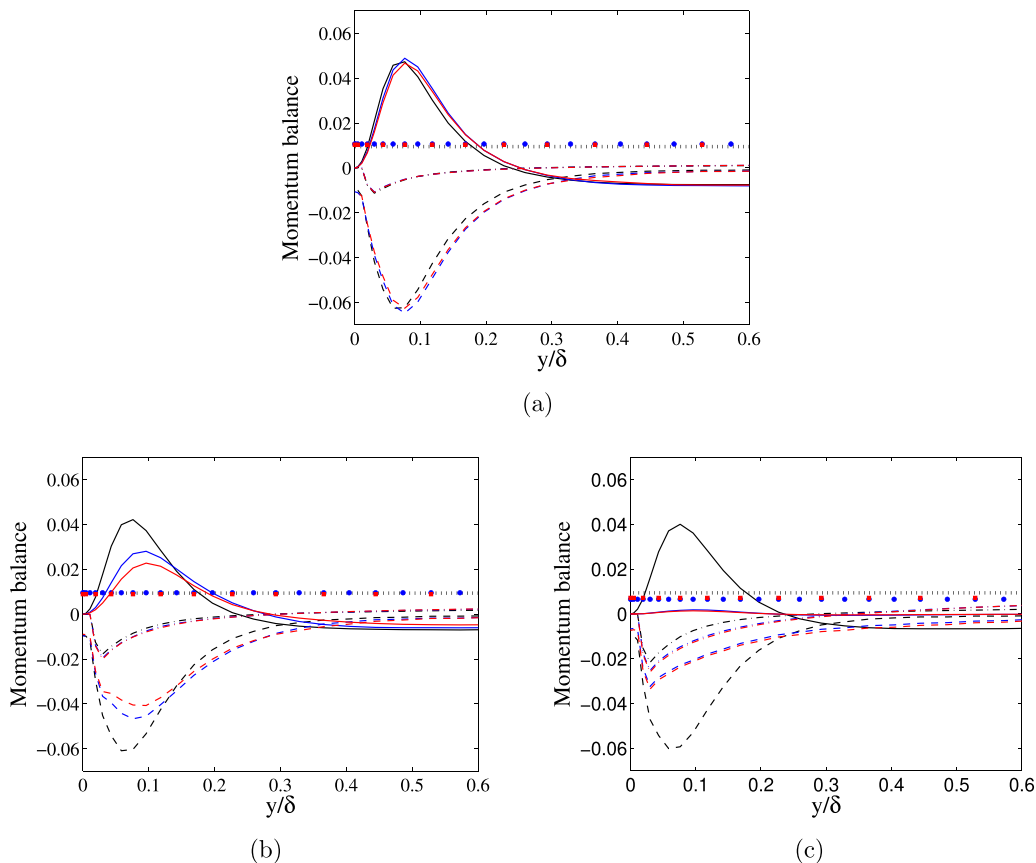
FIG. 10. The terms in fluid momentum equation (14) scaled by $\bar{u}^2/h$ plotted for $\mathrm{Re}_b = 3300$ at (a) $\phi = 0.0003$, (b) $\phi = 0.0005$, and (c) $\phi = 0.0006$. Symbols are as follows: DNS: Black dotted $(-1/\rho_f)d\bar{p}/dx$, black dashed $\nu(d^2\bar{u}_x/dy^2)$, black solid $d\overline{(-u'_x u'_y)}/dy$, black dash-dotted $\overline{\frac{\rho_p f \phi_c}{\rho_f \tau_p}(u_x - v_x)}$. Smagorinsky: Red dotted $(-1/\rho_f)d\overline{\widetilde{p}}/dx$, red dashed $(\nu + \nu_t)d^2\overline{\widetilde{u}}_x/dy^2$, red solid $d\overline{(-\widetilde{u}'_x \widetilde{u}'_y)}/dy$, red dot-dashed $\overline{\frac{\rho_p f \phi_c}{\rho_f \tau_p}(\widetilde{u}_x - \widetilde{v}_x)}$. Dynamic Smagorinsky: Blue dotted $(-1/\rho_f)d\overline{\widetilde{p}}/dx$, blue dashed $(\nu + \nu_t)d^2\overline{\widetilde{u}}_x/dy^2$, blue solid $d\overline{(-\widetilde{u}'_x \widetilde{u}'_y)}/dy$, blue dot-dashed $\overline{\frac{\rho_p f \phi_c}{\rho_f \tau_p}(\widetilde{u}_x - \widetilde{v}_x)}$.

fractions, which is shown in Fig. 10. At low Reynolds number, there is a deviation of less than 20% up to $\phi = 5 \times 10^{-4}$. Beyond that volume fraction deviation increases as models predict drastic turbulence collapse, and there is a sharp change in curvature of the mean flow of the fluid phase.

Similar results are also obtained at moderate Reynolds number ($\mathrm{Re}_b = 5600$). All the components of momentum balance equations are shown in Fig. 11 for different volume fractions. At volume fractions of 1.0×10^{-3} and 1.5×10^{-3}, both the LES models show an underprediction of divergence of Reynolds stress and overprediction of the particle feedback force compared to DNS data. In the case of the dynamic Smagorinsky model, the divergence of Reynolds stress is higher than predicted by the Smagorinsky model, and consequently, it shows a higher critical volume loading, Fig. 11(c). In earlier work, Vreman [6] has decomposed the particle feedback force into a uniform bulk averaged component, a nonuniform local mean component, and a fluctuating component. The nonuniform local mean component is a function of wall-normal distance. The author has performed the simulations at a particle volume loading $\phi \approx 10^{-4}$ in the presence of
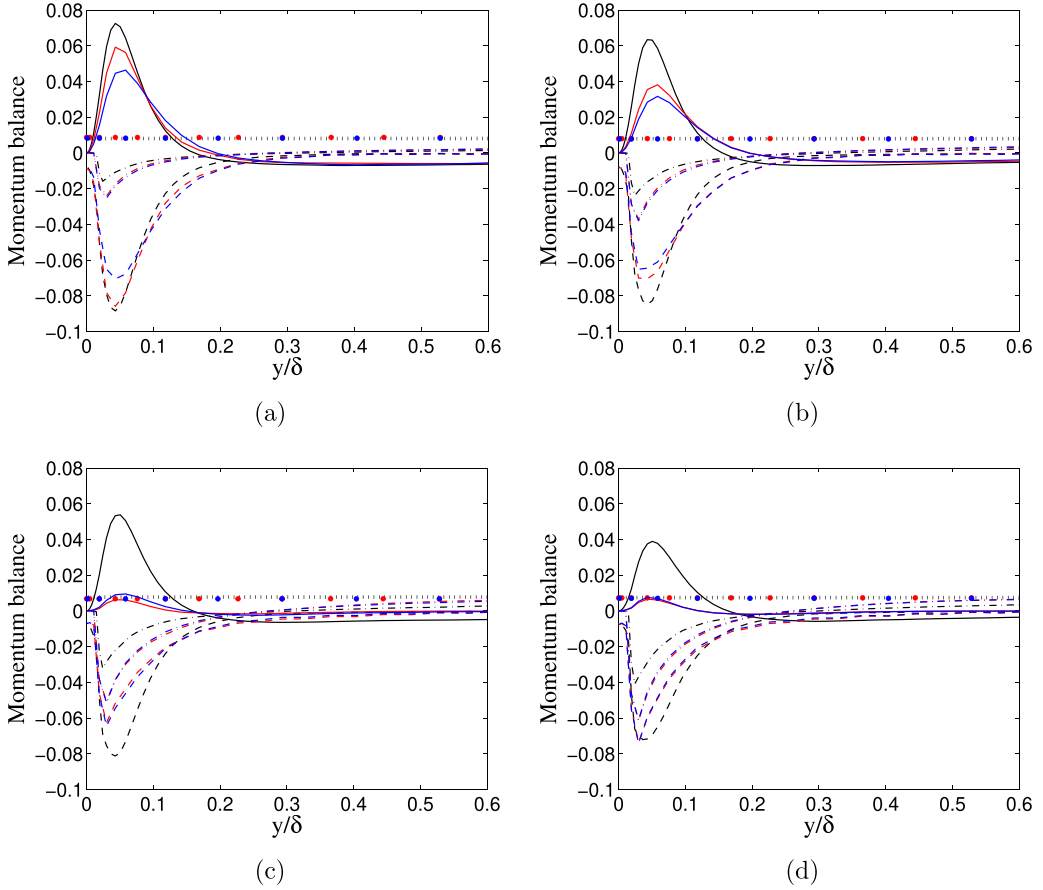
FIG. 11. The terms in fluid momentum equation (14) scaled by $\bar{u}^2/h$ plotted for $Re_b = 5600$ at (a) $\phi = 0.0010$, (b) $\phi = 0.0015$, (c) $\phi = 0.0020$, and (d) $\phi = 0.0025$. Symbols are same as in Fig. 10.

a rough and smooth wall. He observed no significant change in the fluid mean velocity profile, but there is a significant change in nonuniform drag force in the presence of wall roughness, which leads to a variation in Reynolds stress. In the present work, we have performed simulations for a range of volume fractions ($\phi = 10^{-4}$ to 3×10^{-3}) for two different Reynolds numbers using LES and DNS methods. It is observed in Fig. 9 that, in the prediction of relative velocities, there is a difference of 10%–15% at $Re_b = 3300$ and 20%–25% at $Re_b = 5600$ by LES compared to DNS for low volume fractions. The difference is also reflected in the feedback force term in Fig. 10. It may appear that the inaccuracy of LES in predicting the divergence of the Reynolds stress term and consequent underprediction of turbulence collapse is related to the overprediction of the particle induced drag force as reported by Vreman [6]. In our study, we have estimated space averaged values of all the terms that appear in the momentum balance equation and plotted these in Fig. 12. A critical look reveals that, for an increase in the particle volume fraction from 10^{-4} to 5×10^{-4}, the change in the drag force prediction by LES (Smagorinsky model) is $\approx$30% higher compared to DNS. However, the cumulative change in the pressure drop and curvature of the mean velocity profile as predicted by LES is more than one order of magnitude compared to the DNS, which leads to a significant decrease in the divergence of the Reynolds stress term as predicted by LES. The filtered DNS exactly predicts the space averaged viscous term, $\langle D \rangle_s$, similar to the DNS for all the volume fractions (see Fig. 13). At a moderate Reynolds number ($Re_b = 5600$), the dynamic Smagorinsky model predicts a slower decay rate with an increase in volume fraction due to dynamically computed
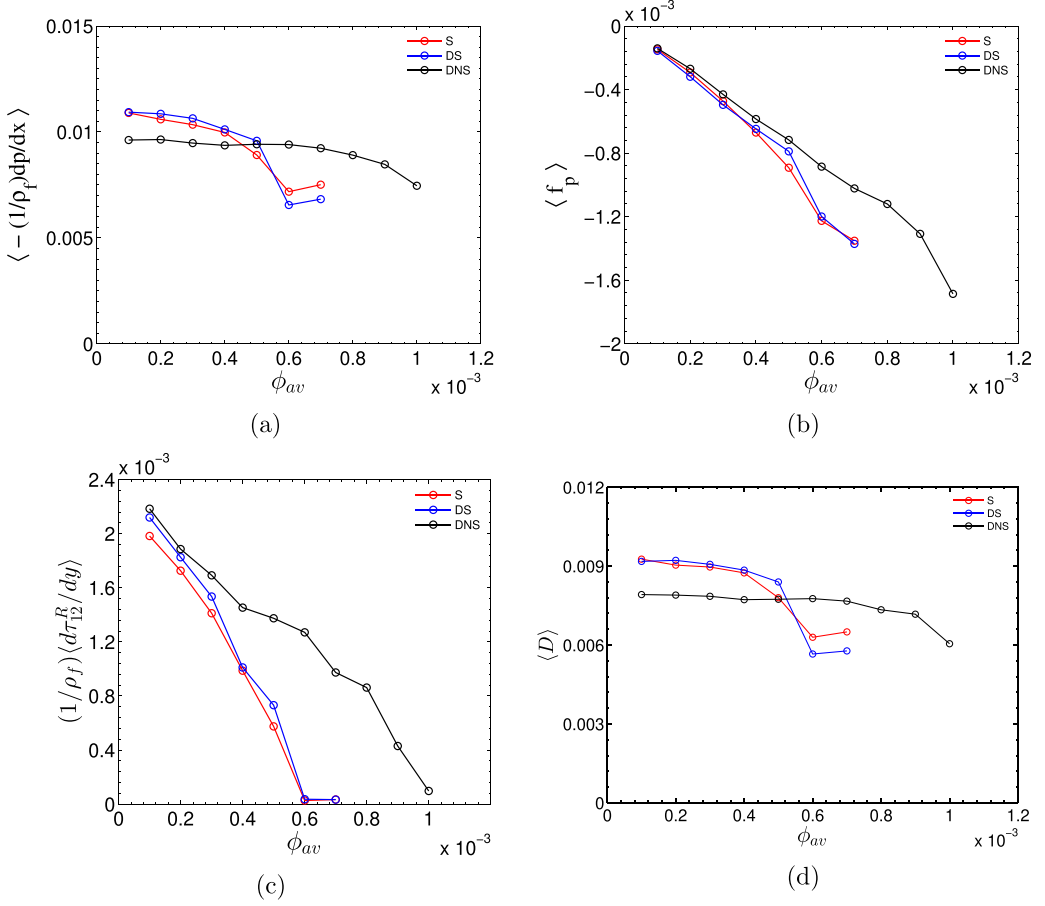
FIG. 12. Averaged momentum balance terms from Eq. (14) across channel width, $y/\delta = 0.05$–1, plotted for range of average volume fractions for Reynolds number of 3300. (a) Pressure gradient, (b) particle feedback term, (c) divergence of Reynolds stress, and (d) viscous diffusion term. S: Smagorinsky model. DS: Dynamic Smagorinsky model. DNS: Direct numerical simulation.

lower C_s value as compared to the Smagorinsky model. Therefore, the failure of the LES models to accurately capture the critical volume loading cannot be merely due to its inability to predict accurate drag force and consequent inaccuracy in the feedback force. The discrepancy may originate due to modeling error with increased anisotropy and low intensity of turbulence fluctuations at higher volume loading. The Smagorinsky and dynamic Smagorinsky models may not be able to properly capture the generation of vortical structures and self-sustaining mechanism of turbulence. Further study is required to address this issue.

E. Fluid phase energy balance

The filtered kinetic energy equation of the mean flow in the stationary state can be described as

$$-\widetilde{U}_x \frac{1}{\rho}\frac{\partial \widetilde{P}}{\partial x} - \frac{\partial (\overline{\widetilde{u'_x u'_y}}\widetilde{U}_x)}{\partial y} + \overline{\widetilde{u'_x u'_y}}\frac{\partial (\widetilde{U}_x)}{\partial y} + (\nu + \nu_t)\frac{\partial}{\partial y}\left(\widetilde{U}_x \frac{\partial \widetilde{U}_x}{\partial y}\right) - (\nu + \nu_t)\frac{\partial \widetilde{U}_x}{\partial y}\frac{\partial \widetilde{U}_x}{\partial y}$$

$$-\widetilde{U}_x \overline{\frac{\rho_p f \phi}{\rho_f \tau_p}}(\widetilde{u}_x - \widetilde{v}_x) = 0. \tag{16}$$
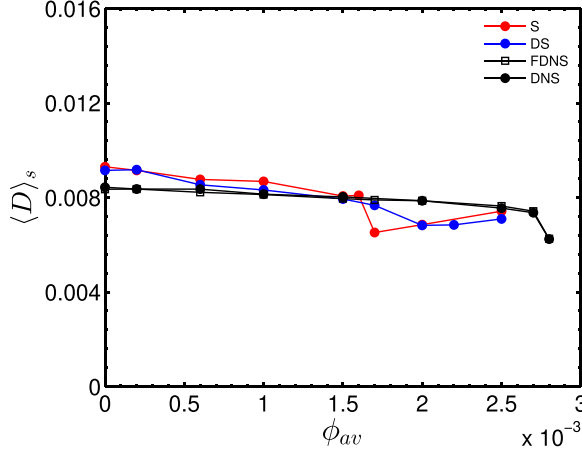
FIG. 13. The diffusion term (D) averaged across the channel width from Eq. (14) plotted for a range of average volume fractions (ϕ_{av}) for $Re_b = 5600$. S: Smagorinsky model. DS: Dynamic Smagorinsky model. DNS: Direct numerical simulation. FDNS: Filtered DNS.

In Eq. (16), the first term is the energy due to pressure work, the second and fourth terms are the divergence of energy fluxes due to Reynolds stress and fluid viscous stress, respectively, the third term is the turbulent production, the fifth term is the viscous dissipation due to mean shear, and the sixth term is the loss of energy due to the particle drag. The filtered kinetic energy balance for the turbulent fluctuations is written as

$$\widetilde{u_i'} \widetilde{u_j'} \frac{\partial \widetilde{U}_i}{\partial x_j} = -\frac{1}{2} \frac{\partial \overline{(\widetilde{u_i'} \widetilde{u_i'} \widetilde{u_j'})}}{\partial x_j} - \frac{1}{\rho} \frac{\partial \overline{(\widetilde{p'} \widetilde{u_i'})}}{\partial x_i} + (\nu + \nu_t) \overline{\frac{\partial}{\partial x_j} \left(\widetilde{u_i'} \frac{\partial \widetilde{u_i'}}{\partial x_j} \right)}$$

$$- (\nu + \nu_t) \overline{\frac{\partial \widetilde{u_i'}}{\partial x_j} \frac{\partial \widetilde{u_i'}}{\partial x_j}} - \frac{\rho_p f \phi_c}{\rho_f \tau_p} \overline{(\widetilde{u_i'} \widetilde{u_i'} - \widetilde{v_i'} \widetilde{u_i'})}, \tag{17}$$

where the first three terms on the right-hand side are the flux terms, the fourth term is the viscous dissipation of turbulent kinetic energy, and the last term is the change in turbulent kinetic energy due to the particle-fluid interaction at fluctuating scales. When Eqs. (16) and (17) are averaged spatially in the wall-normal direction, the flux term becomes zero due to no-slip condition at the walls, and the equations are represented as

$$-\widetilde{U}_x \frac{1}{\rho_f} \frac{\partial \widetilde{P}}{\partial x} + \left\langle \overline{\widetilde{u_x'} \widetilde{u_y'}} \frac{\partial (\widetilde{U}_x)}{\partial y} \right\rangle_s - (\nu + \nu_t) \left\langle \frac{\partial \widetilde{U}_x}{\partial y} \frac{\partial \widetilde{U}_x}{\partial y} \right\rangle_s - \left\langle \widetilde{U}_x \overline{\frac{\rho_p f \phi_c}{\rho_f \tau_p}} (\widetilde{u}_x - \widetilde{v}_x) \right\rangle_s = 0, \tag{18}$$

$$-\left\langle \overline{\widetilde{u_i'} \widetilde{u_j'}} \frac{\partial \widetilde{U}_i}{\partial x_j} \right\rangle_s - (\nu + \nu_t) \left\langle \overline{\frac{\partial \widetilde{u_i'}}{\partial x_j} \frac{\partial \widetilde{u_i'}}{\partial x_j}} \right\rangle_s - \left\langle \frac{\rho_p f \phi_c}{\rho_f \tau_p} \overline{(\widetilde{u_i'} \widetilde{u_i'} - \widetilde{v_i'} \widetilde{u_i'})} \right\rangle_s = 0. \tag{19}$$

The terms in the energy balance equations are scaled by $\bar{u}^3 / 2\delta$. The mean pressure work (I), mean viscous dissipation (ϵ_m), and mean dissipation due to the particle drag (T) in Eq. (18) are significant. In Eq. (19), the transport of energy from the mean flow to the fluctuations due to Reynolds stress and viscous dissipation of fluctuating kinetic energy are comparable in magnitude close to the wall, while dissipation of fluctuating energy due to particles is smaller. The terms of the energy balance equation for moderate Reynolds number ($Re_b = 5600$) are shown in Figs. 14 and 15. It is observed that both the LES models underpredict the viscous dissipation at mean flow scale, turbulence production, and viscous dissipation at fluctuating scale. However, dissipation due to the particle drag is overpredicted. The Smagorinsky model is closer to DNS than dynamic Smagorinsky
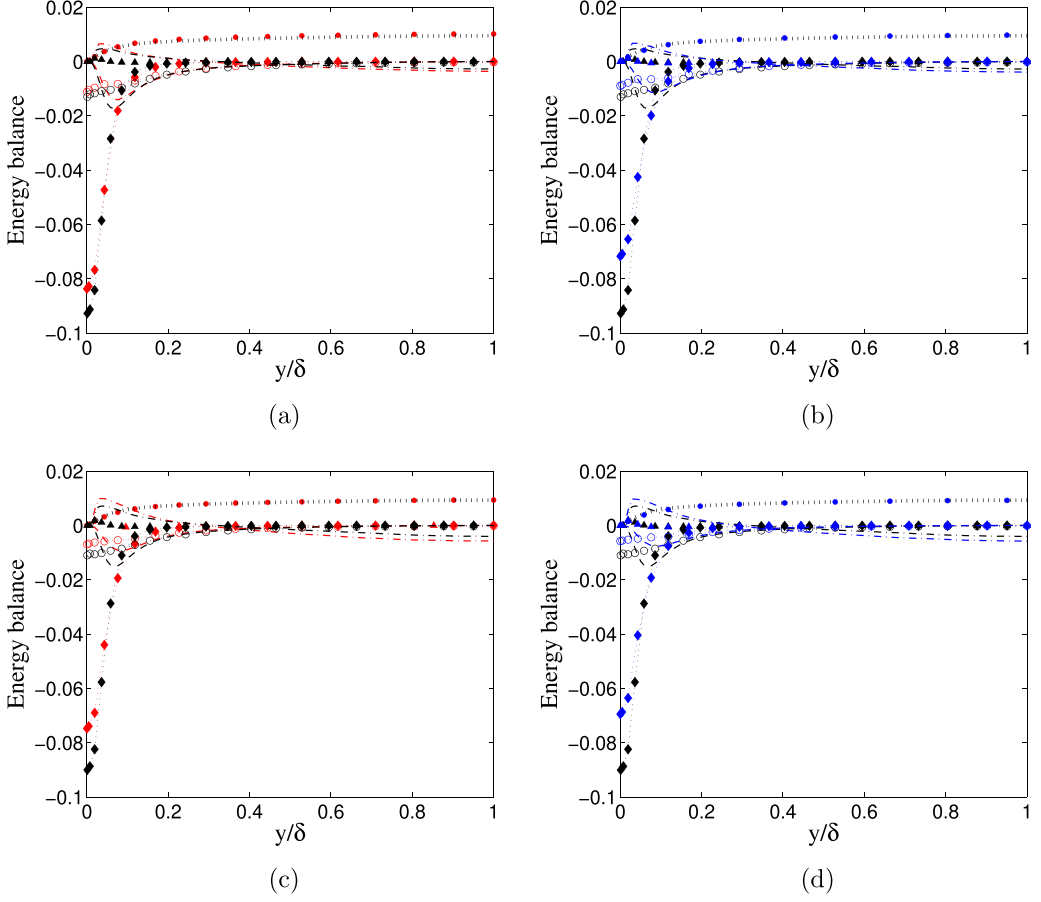
FIG. 14. The terms in fluid energy equations (18) and (19) scaled by $\bar{u}^3/h$ plotted for $\mathrm{Re}_b = 5600$. DNS: Black dotted $(-(1/\rho_f)\bar{u}_x d\bar{p}/dx)$, black diamonds $\nu(d\bar{u}_x/dy)^2$, black dashed $\overline{u'_x u'_y} d\bar{u}_x/dy$, black dot-dashed $(-\widetilde{u}_x \frac{\rho_p f\phi}{\rho\tau_p}(\widetilde{u}_x - \widetilde{v}_x))$, black circles $\nu[\overline{\nabla u' : (\nabla u')^T}]$, black triangles $(-\frac{\rho_p f\phi_c}{\rho\tau_p}\overline{(u'_i u'_i - v'_i u'_i)})$. Smagorinsky: Red dotted $(-(1/\rho_f)\widetilde{\bar{u}}_x d\widetilde{\bar{p}}/dx)$, red diamonds $(\nu + \nu_t)(d\widetilde{\bar{u}}_x/dy)^2$, red dashed $\widetilde{u'_x u'_y} d\widetilde{\bar{u}}_x/dy$, red dot-dashed $(-\widetilde{u}_x \frac{\rho_p f\phi}{\rho\tau_p}(\widetilde{u}_x - \widetilde{v}_x))$, red circles $(\nu + \nu_t)[\overline{\nabla \widetilde{u'} : (\nabla \widetilde{u'})^T}]$, red triangles $(-\frac{\rho_p f\phi_c}{\rho\tau_p}\overline{(\widetilde{u'_i u'_i} - \widetilde{v'_i u'_i})})$. Symbols for dynamic Smagorinsky model are same as used for Smagorinsky model with blue color. (a) $\phi = 0.0010$, (b) $\phi = 0.0010$, (c) $\phi = 0.0015$, and (d) $\phi = 0.0015$.

until turbulence is collapsed for this model, Figs. 14(a)–14(d). There is no significant variation in the mean pressure energy from $\phi = 1 \times 10^{-3}$ to $\phi = 1.5 \times 10^{-3}$ as shown in Figs. 14(a)–14(d). At higher volume loadings [Figs. 15(a)–15(d)], turbulent production and viscous dissipation at fluctuating scales are almost zero for LES models. The dissipation due to particle-fluid interaction in the fluctuating kinetic energy is negligible for all the volume loadings. It is observed that, at the critical loadings predicted by both the LES models, there is a sudden decrease in turbulence production but mean particle-induced dissipation does not show any abrupt increase. Direct numerical simulations also reveal a similar collapse in turbulence (Fig. 3). However, the critical volume loading is underpredicted by the LES models compared to DNS. Similar observations are also followed at a lower Reynolds number. However, the figures are not shown here for the sake of brevity. All the significant terms in the energy equations for mean flow and fluctuating energy equation are predicted well compared to DNS results at the bulk Reynolds number of 3300 and with low volume loading
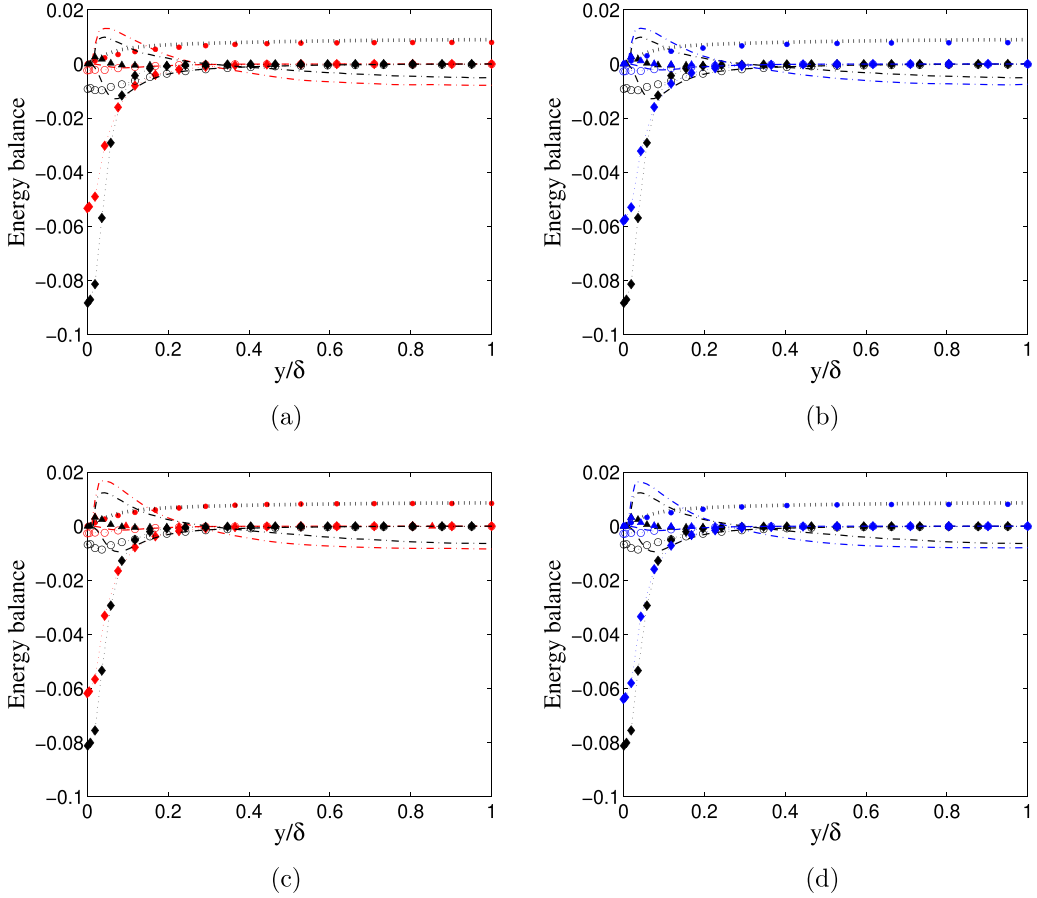
FIG. 15. The terms in fluid energy equations (18) and (19) scaled by $\bar{u}^3/h$ plotted for $Re_b = 5600$. The symbols are same as in Fig. 14. (a) $\phi = 0.0020$, (b) $\phi = 0.0020$, (c) $\phi = 0.0025$, and (d) $\phi = 0.0025$.

($\phi = 3 \times 10^{-4}$). A maximum deviation of 5% is observed. With an increase in the particle volume loading, there is a significant underprediction of the "turbulence production term" by the models, and consequently, both the models show an early collapse of turbulence. To understand the reason of the discrepancy in the prediction of CPVL by LES models, we estimate the average of viscous dissipation, dissipation due to the particle drag, and the pressure work term across the channel using Eq. (18) and plot as a function of the particle volume loading.

Figures 16(a) and 16(b) show all the averaged terms for two different Reynolds numbers. Both the LES models overpredict the average of the viscous dissipation term at low volume fraction. A steady decrease is observed with an increase in volume fraction as eddy viscosity decreases. The Smagorinsky model shows a sharp decrease at a moderate Reynolds number, but the dynamic Smagorinsky model does not. Figures 16(a) and 16(b) also show the total dissipation term (referred as "sum" in the figures). It is observed that all the components of energy other than the pressure work are predicted well by the models till the critical point. Both the models predict a higher pressure work term at low volume fractions, which is consistent with a marginally higher turbulence production term. The LES models predict erroneously that, at a volume fraction of 6×10^{-4} (at $Re_b = 3300$), there is a drastic drop in pressure work, turbulence production, and dissipation terms. The dissipation due to particle drag increases at this point. The *difference* between the energy input through pressure work and total dissipation, which is utilized for turbulence production, decreases
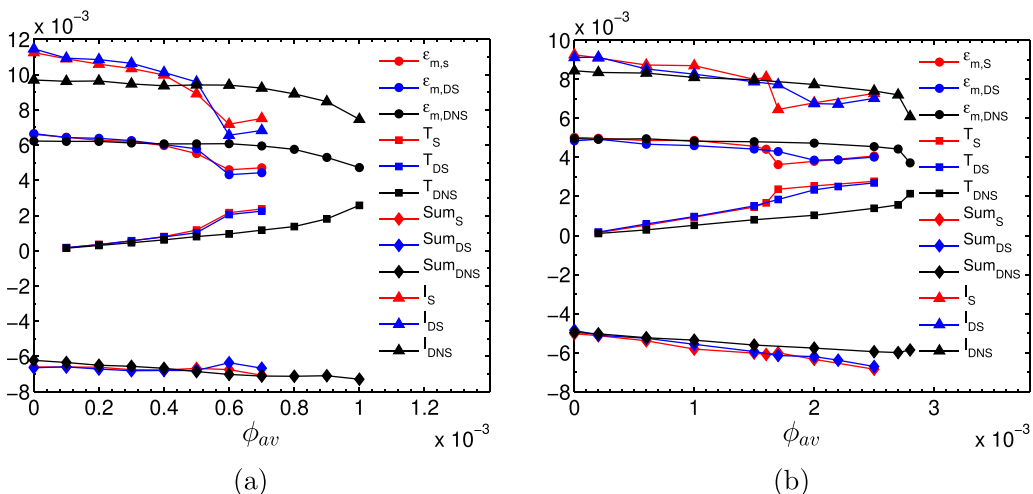
FIG. 16. The average of terms from Eq. (18) for (a) $Re_b = 3300$ and (b) $Re_b = 5600$ are mean viscous dissipation (ϵ_m), dissipation due to particle drag (T), sum $= -(\epsilon_m + T)$, and I is input energy from pressure work plotted for range of volume fractions (ϕ_{av}). Color as follows: Red: Smagorinsky model (S). Blue: Dynamic Smagorinsky model (DS). Black: Direct numerical simulation (DNS).

discontinuously as shown in Figs. 17(a) and 17(b). However, such an observation does not confirm that the drastic decrease in turbulence production originates due to the reduction in pressure work. Due to a drastic drop in the pressure work and the turbulence production, the flow becomes laminar with a constant fluid volumetric flow rate. It should be noted that, for this study, the resolution in the volume fraction is 10^{-4} and the collapse in turbulence has been captured with such a small change in volume fraction. It is shown in Fig. 16 that the deviation in total dissipation (which appears in the mean energy balance equation) compared to DNS is much smaller than the deviation in pressure work and the production term (shown in Fig. 18). The ratios of production terms predicted by LES models to that predicted by DNS are presented in Figs. 18(a) and 18(b) for both the Reynolds numbers. It is observed that the models erroneously predict the turbulence collapse when
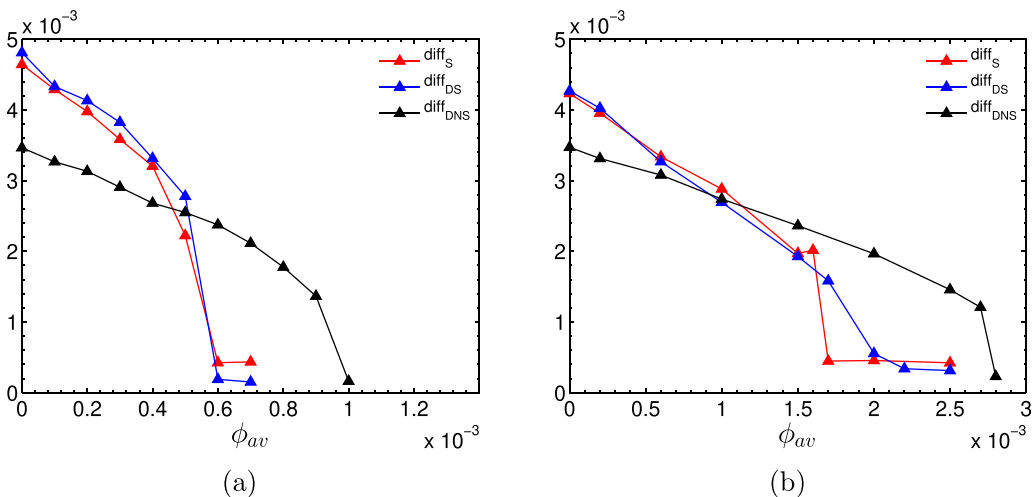

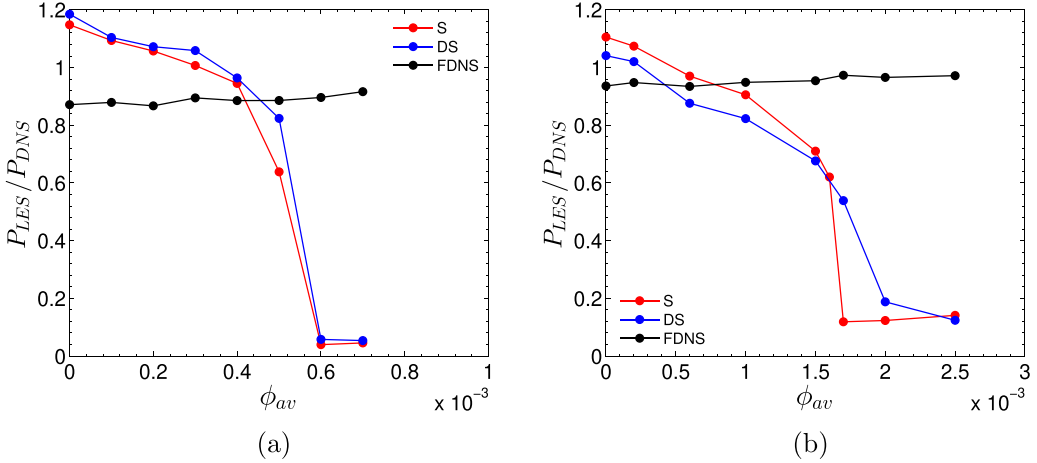FIG. 17. diff $= I - (\epsilon_m + T)$ for (a) $Re_b = 3300$ and (b) $Re_b = 5600$. For symbols see Fig. 16.

FIG. 18. The ratio of production term (P) from Eq. (18) predicted by LES models with respect to DNS plotted against average volume fractions (ϕ_{av}) for (a) $\mathrm{Re}_b = 3300$, (b) $\mathrm{Re}_b = 5600$. S: Smagorinsky model. DS: Dynamic Smagorinsky model. FDNS: Filtered direct numerical simulation.

the model prediction of $P_{\mathrm{LES}}/P_{\mathrm{DNS}}$ becomes less than approximately 60%. To understand whether the underprediction of CPVL by LES models originates due to the application of filter on the fluid phase velocity field, we compute the turbulence productions at all the volume fractions by applying a similar filter on the DNS data, which is shown in Figs. 18(a) and 18(b). The figures interestingly depict that the ratios of the production computed by filtered DNS (FDNS) to that computed by DNS do not show any decrease with an increase in volume fraction. It is worth noting that, with the increase in volume loading, the anisotropy in the fluid fluctuations increases, and also, the intensities of all the components of fluid fluctuations decrease. It is shown in Figs. 3(a) and 3(b) that there is an increase in anisotropy (ratio of the second moment of streamwise fluctuation to wall-normal fluctuation) by 1.5 times for the volume loading 5×10^{-4} compared to the unladen flow. Therefore, it is expected that there will be an inaccurate prediction of the production term if the LES models are not robust enough to capture the vortical structures associated with the low amplitude wall-normal and spanwise fluctuations at higher volume loading.

To obtain further insight about the turbulence collapse by LES models, we perform a set of simulations to compute the temporal evolution of the domain averaged second moments of the fluid velocity fluctuations at different solid volume fractions and present these in Fig. 19. We use the data from the stationary state of the fluid only phase simulations as the initial condition. The temporal values of the second moment of fluctuations are normalized with the second moment of the unladen simulation. A similar computation is performed using the FDNS technique for volume fraction 5.5×10^{-4} and shown in Fig. 19(e). It should be noted that the figures show the initial trend of the evolution of fluid fluctuations; the particle-laden flows do not reach the stationary state within the time duration shown in the figures. However, the initial trend carries the signature of the turbulence collapse. It is depicted that, in all cases, wall-normal fluid velocity fluctuations decay faster than the streamwise fluctuations and the decay rates predicted by the LES models are higher than the DNS prediction. It is shown in the figure that, when the particle volume fraction becomes 5.5×10^{-4}, the wall-normal velocity fluctuations predicted by LES models become very low within a time duration of 200 [Fig. 19(c)]. It is observed that the streamwise fluctuation for the Smagorinsky model decays faster at this volume loading compared to the dynamic model. The Smagorinsky model predicts a turbulence collapse at this point; the dynamic model shows the collapse at a little higher volume fraction of 6.0×10^{-4}. To understand whether the early decays predicted by the LES models happen due to the effect of filtering, we calculate all the second moments of the fluctuations
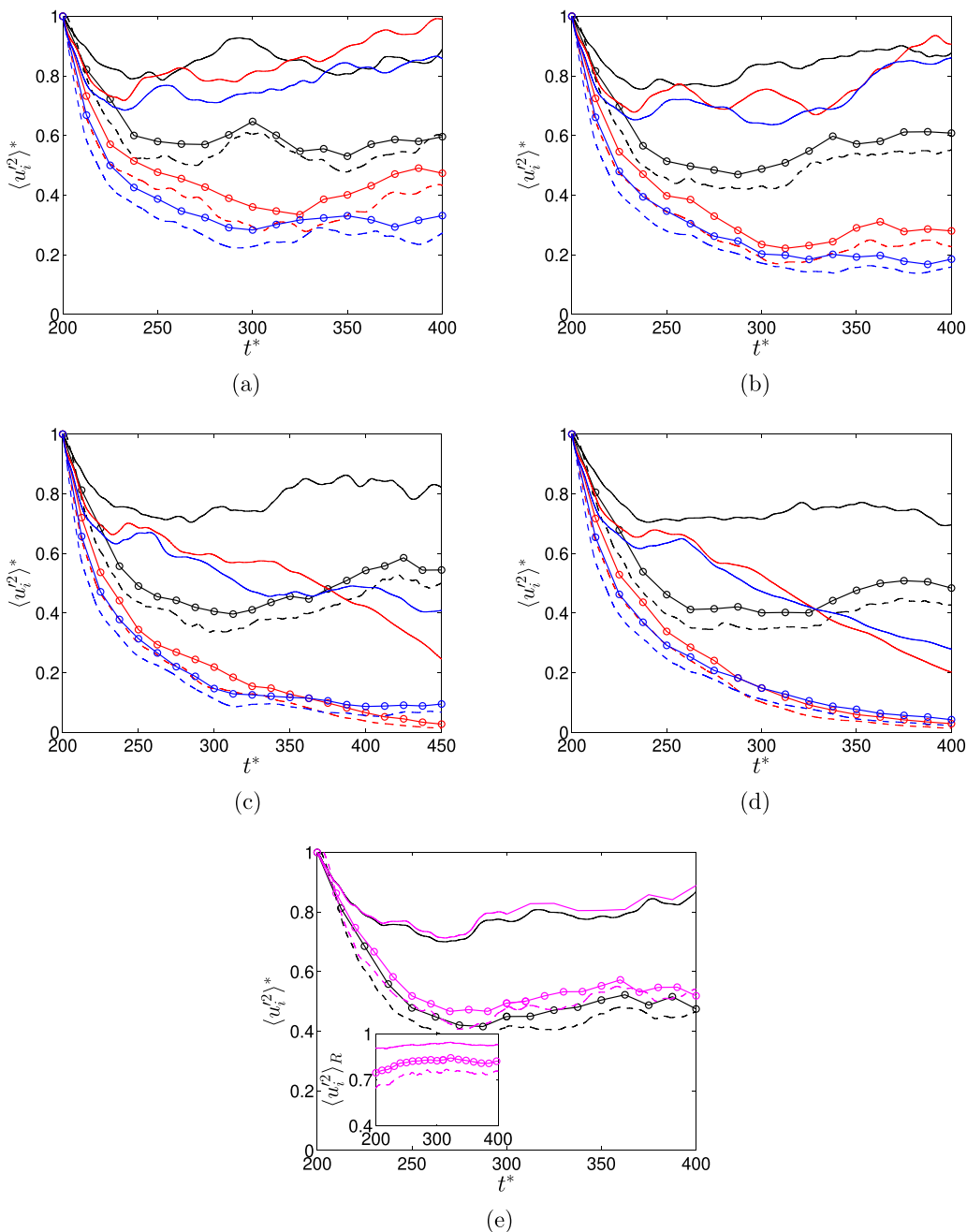
FIG. 19. Sum of square of fluid fluctuations (normalized with $t^* = 200$ value) over time evolution for different volume fractions at $Re_b = 3300$. Colors are as follows: Red, Smagorinsky model; blue, dynamic Smagorinsky model; black, DNS; pink, FDNS. Solid lines, streamwise; dashed lines, wall-normal; solid lines with circle symbols, spanwise component. Also, t^* is normalized with half-channel width and average fluid velocity. (a) $\phi = 0.0004$, (b) $\phi = 0.0005$, (c) $\phi = 0.00055$, (d) $\phi = 0.0006$, (e) $\phi = 0.00055$. In the inset figure of Fig. 19(e), the FDNS data is normalized with DNS data.

using filtered DNS (FDNS) data as shown in Fig. 19(e). It is shown that the filtered data show a decay which is very similar to the DNS. Also, we simulate three hypothetical situations by controlling the particle feedback forces on the fluid phase. In the first case, we consider that the particle exerts no feedback force in the wall-normal (y) direction, but the magnitude of spanwise and streamwise feedback forces are unaltered; in the second case, we switch off the feedback force in the y and z directions but consider an unaltered streamwise feedback force; and in the third case, we reduce the streamwise feedback force by 30% (which is the maximum deviation from DNS in relative velocity). It is observed that there are no change in CPVL$_{\text{LES}}$ from the earlier value for the first case, but in the second and third cases, there is a marginal increase of CPVL$_{\text{LES}}$ from 5.5×10^{-4} to 7×10^{-4}. It should be noted that CPVL$_{\text{LES}} = 7 \times 10^{-4}$ is also much lower than that predicted by DNS, CPVL$_{\text{DNS}} = 1.0 \times 10^{-3}$.

Therefore, all these observations suggest that the underprediction of the critical volume loading (CPVL) by the LES models may originate due to the subgrid scale modeling error and the inability of the models to capture the vortical structure and self-sustaining turbulence generation mechanism at high particle loading, but not due to the filtering error or inaccuracy in predicting the drag force on the particles. Further investigation on the prediction of coherent structure and their breakdown to generate vorticity by the LES technique is left as a future scope.

In summary, two extensively used LES models, the Smagorinsky and dynamic Smagorinsky models, predict the turbulence attenuation reasonably well for a range of volume fraction and Reynolds numbers. The LES models also capture the drastic collapse of the turbulence fluctuations. However, the critical volume loading at which the collapse happens is underpredicted by the LES models. For an accurate prediction of CPVL and turbulence modulation, the models not only require predicting the diffusion and viscous dissipation accurately but also the production of turbulent kinetic energy. In the case of the Smagorinsky model, C_s is an input parameter which may require modification due to the presence of particles. The dynamic model also fails to accurately predict CPVL, although, in this technique, C_s is calculated locally with the evolution of the flow. The detailed analysis presented in this paper suggests that further investigation is required on the modification of the inertial range of spectra and Kolmogorov constant due to particle loading. Also, an assessment of the capability of the LES models to capture the coherent structures and their breakdown at high particle concentration needs to be addressed.

IV. CONCLUSIONS

The present work reports a critical assessment of the applicability of two widely used LES models (the Smagorinsky and dynamic Smagorinsky model) in predicting turbulence modulation for the particle-laden flows. The results are reported for two different Reynolds numbers (Re$_b = 3300$ and 5600) and a wide range of volume fraction. Effects of the particle-particle and particle-wall interactions have also been considered. An analysis of the averaged second moments of fluid velocity fluctuations shows that LES models can predict those with an accuracy of more than 80% for volume fractions lower than the critical volume fraction. Although both the models predict the increase in turbulent attenuation with increasing volume fraction, the deviation in the predicted value compared to DNS results increases. Both the LES models underpredict the critical particle volume loading (CPVL) at which turbulence collapses.

The sources of the discrepancy in the LES prediction compared to DNS may be the inaccurate prediction of feedback force and consequent high particle-induced dissipation or the underprediction of turbulence production. To estimate the error due to inaccuracy in drag prediction, we calculate the distribution function of the relative velocity and compute all the terms appear in the momentum balance equation. A statistical analysis of the relative velocity distribution shows that the distribution functions are qualitatively similar to the DNS. At low Reynolds number, a maximum deviation of 15% in the mean relative velocity is observed for volume fractions lower than CPVL, whereas at moderate Reynolds number, the maximum deviation is around 25% before the turbulence collapses

for LES models. Similarly, we find a maximum deviation of 25% compared to DNS results in the feedback force term at a volume loading which corresponds to $CPVL_{LES}$.

All the significant terms which appear in the energy balance equations have been computed for different volume loadings. It is observed that the energy dissipation due to particle drag is much lower than the viscous dissipation at the mean scale. The total dissipation does not vary significantly from the DNS value, but the energy input due to pressure work and the turbulence production drop drastically.

To understand whether the early decays predicted by the LES models happen due to filtering, we have calculated all the second moments of the fluctuations using filtered-DNS (FDNS) data. It is observed that the filtered data show a decay which is very much similar to that predicted by DNS. To check whether the difference in the prediction of particle feedback force and particle induces dissipation by LES models is responsible for the early collapse of turbulence, we have hypothetically reduced the extent of feedback force in LES simulations to predict the critical volume loading. Such a numerical experiment reveals that $CPVL_{LES}$ is marginally increased for 30% reduction in streamwise drag force. Therefore, all these observations suggest that the underprediction of the
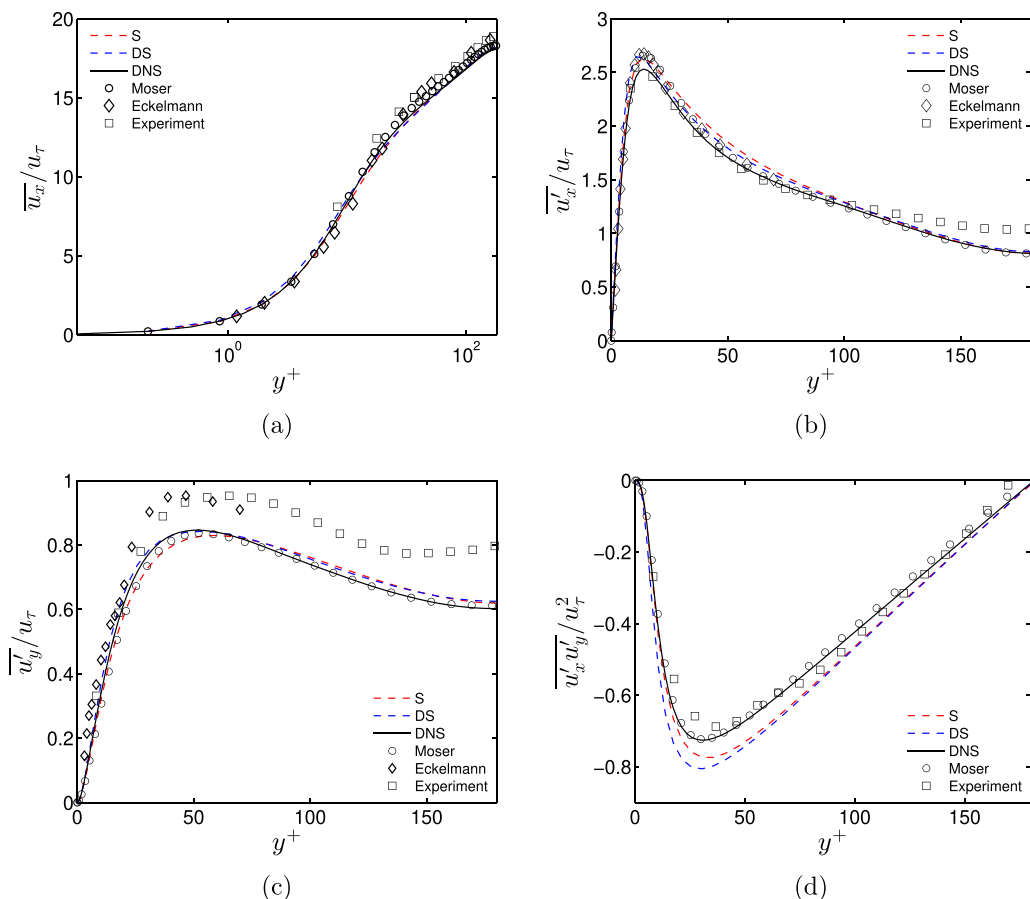

FIG. 20. The unladen (a) streamwise mean velocity, (b) streamwise fluid fluctuations, (c) wall-normal fluctuations, and (d) cross-stream stress normalized by frictional velocity (u_τ) at $Re_b = 5600$. y^+ is wall-normal distance normalized by viscous scales. S: Smagorinsky model. DS: Dynamic Smagorinsky model. DNS: Direct numerical simulation. DNS data from Moser [55]; experimental data from Eckelmann [54]. "Experiment" shows the laboratory experimental results at $Re_b = 6500$.

critical volume loading (CPVL) by the LES models may originate due to the subgrid scale modeling error and the inability of the models to capture the vortical structure and self-sustaining turbulence generation mechanism at high particle loading, but not due to the filtering error or inaccuracy in predicting the drag force on the particles. Further investigation on the prediction of coherent structure and their breakdown to generate vorticity by the LES technique is left as a future scope. It is to be noted that the present study is performed at low and moderate Reynolds numbers. The range of volume fraction over which LES performs better may increase with increase in Reynolds number, which is left as a future scope.

ACKNOWLEDGMENTS

APPENDIX: VALIDATION

Mean fluid phase velocity and the root mean square velocity fluctuations obtained for unladen flow using the Smagorinsky and dynamic Smagorinsky models are compared with DNS for $Re_b = 5600$. In case of the Smagorinsky model, $C_s = 0.125$ is used. The mean velocity profile is shown in Fig. 20(a). The mean profile predicted by the Smagorinsky model and dynamic Smagorinsky model matches well with DNS. The rms of streamwise fluctuations is also predicted well by both the LES models by a maximum difference of 5% at the peak location, Fig. 20(b). The rms of wall-normal fluctuations matches well with DNS results. There is a difference of less than 10% at the peak value of Reynolds stress. We have also included DNS data Moser *et al.* [55], experimental data by Eckelmann [54], and also data generated by in-house experiments performed at $Re_b = 6500$. LES results also show good agreement with the experimental data.

[1] Y. Yamamoto, M. Potthoff, T. Tanaka, T. Kajishima, and Y. Tsuji, Large-eddy simulation of turbulent gas particle flow in a vertical channel: Effect of considering inter-particle collisions, J. Fluid Mech. **442**, 303 (2001).

[2] J. K. Eaton and J. R. Fessler, Preferential concentration of particles by turbulence, Int. J. Multiphase Flow **20**, 169 (1994).

[3] K. D. Squires and J. K. Eaton, Preferential concentration of particles by turbulence, Phys. Fluids **3**, 1169 (1991).

[4] M. Boivin, O. Simonin, and K. D. Squires, On the prediction of gas-solid flows with two-way coupling using large eddy simulation, Phys. Fluids **12**, 2080 (2000).

[5] G. Mallouppas and B. van Wachem, Large eddy simulations of turbulent particle-laden channel flow, Int. J. Multiphase Flow **54**, 65 (2013).

[6] A. Vreman, Turbulence attenuation in particle-laden flow in smooth and rough channels, J. Fluid Mech. **773**, 103 (2015).

[7] J. D. Kulick, J. R. Fessler, and J. K. Eaton, Particle response and turbulence modification in fully developed channel flow, J. Fluid Mech. **277**, 109 (1994).

[8] T. Kajishima, S. Takiguchi, H. Hamasaki, and Y. Miyake, Turbulence structure of particle laden flow in a vertical plane channel due to vortex shedding, JSME Int. J., Ser. B **44**, 526 (2001).

[9] F. Coletti, M. Toloui, K. O. Fong, A. Nemes, and L. Baker, Volumetric distribution and velocity of inertial particles in a turbulent channel flow, in *18th International Symposium on Application of Laser and Imaging Techniques to Fluid Mechanics, Lisbon, Portugal* (Instituto Superior Técnico, Lisbon, 2016).

[10] B. Vreman, B. J. Geurts, N. G. Deen, J. A. M. Kuipers, and J. G. M. Kuerten, Two and four way coupled Eulerian Lagrangian large-eddy simulation of turbulent particle-laden channel flow, Flow, Turbul. Combust. **82**, 47 (2009).

[11] Y. Li, J. B. McLaughlin, K. Kontomaris, and L. Portela, Numerical simulation of particle-laden turbulent channel flow, Phys. Fluids **13**, 2957 (2001).

[12] P. Muramulla, A. Tyagi, P. Goswami, and V. Kumaran, Disruption of turbulence due to particle loading in a dilute gas-particle suspension, J. Fluid Mech. **889**, A28 (2020).

[13] M. Breuer and M. Alletto, Efficient simulation of particle-laden turbulent flows with high mass loadings using LES, Int. J. Heat Fluid Flow **35**, 2 (2012).

[14] A. Vreman, Turbulence characteristics of particle-laden pipe flow, J. Fluid Mech. **584**, 235 (2007).

[15] M. Riella, R. Kahraman, and G. R. Tabor, Reynolds-averaged two-fluid model prediction of moderately dilute fluid-particle flow over a backward-facing step, Int. J. Multiphase Flow **106**, 95 (2018).

[16] S. Dasgupta, R. Jackson, and S. Sundaresan, Gas-particle flow in vertical pipes with high mass loading of particles, Powder Technol. **96**, 6 (1998).

[17] S. Laín, M. Sommerfeld, and J. Kussin, Experimental studies and modelling of four-way coupling in particle-laden horizontal channel flow, Int. J. Heat Fluid Flow **23**, 647 (2002).

[18] P. S. Goswami and V. Kumaran, Particle dynamics in a turbulent particle-gas suspension at high Stokes number. Part 1. Velocity and acceleration distributions, J. Fluid Mech. **646**, 59 (2010).

[19] V. Kumaran, N. Muramulla, A. Tyagi, and P. Goswami, Turbulence collapses at a threshold particle loading in a dilute particle-gas suspension, Europhys. Lett. **128**, 64001 (2020).

[20] P. S. Goswami and V. Kumaran, Particle dynamics in the channel flow of a turbulent particle gas suspension at high Stokes number. Part 1. DNS and fluctuating force model, J. Fluid Mech. **687**, 1 (2011).

[21] C. D. Dritselis, Direct numerical simulation of particle-laden turbulent channel flows with two- and four-way coupling effects: Budgets of Reynolds stress and streamwise enstrophy, Fluid Dyn. Res. **48**, 015507 (2016).

[22] S. Ghosh and P. Goswami, A statistical analysis of velocity and acceleration fluctuations of inertial particles in particle-laden turbulent Couette flow, Phys. Fluids **34**, 015103 (2022).

[23] J. Smagorinsky, General circulation experiments with the primitive equations: I. The basic experiment, Mon. Weather Rev. **91**, 99 (1963).

[24] J. W. Deardorff, The use of subgrid transport equations in a three-dimensional model of atmospheric turbulence, J. Fluids Eng. **95**, 429 (1973).

[25] M. Breuer and F. Hoppe, Influence of a cost-efficient Langevin subgrid-scale model on the dispersed phase of large-eddy simulations of turbulent bubble-laden and particle-laden flows, Int. J. Multiphase Flow **89**, 23 (2017).

[26] J. W. Deardorff, A numerical study of three-dimensional turbulent channel flow at large Reynolds numbers, J. Fluid Mech. **41**, 453 (1970).

[27] V. M. Canuto and Y. Cheng, Determination of the Smagorinsky-Lilly constant Cs, Phys. Fluids **9**, 1368 (1997).

[28] J. Jiménez, On why dynamic subgrid-scale models work, Annual Research Briefs, Center for Turbulence Research, Stanford, CA, 1995.

[29] C. Fureby, A. Gosman, G. Tabor, H. Weller, N. Sandham, and M. Wolfshtein, Large eddy simulation of turbulent channel flows, in *Eleventh Symposium on Turbulent Shear Flows, Grenoble, France* (Institut National Polytechnique de Grenoble, 1997).

[30] J. G. M. Kuerten and A. W. Vreman, Can turbophoresis be predicted by large-eddy simulation? Phys. Fluids **17**, 011701 (2005).

[31] J. G. M. Kuerten, Subgrid modeling in particle-laden channel flow, Phys. Fluids **18**, 025108 (2006).

[32] C. Marchioli, M. V. Salvetti, and A. Soldati, Appraisal of energy recovering sub-grid scale models for large-eddy simulation of turbulent dispersed flows, Acta Mech. **201**, 277 (2008).

[33] C. Marchioli, M. V. Salvetti, and A. Soldati, Some issues concerning large-eddy simulation of inertial particle dispersion in turbulent bounded flows, Phys. Fluids **20**, 040603 (2008).

[34] S. Stolz, N. A. Adams, and L. Kleiser, An approximate deconvolution model for large-eddy simulation with application to incompressible wall-bounded flows, Phys. Fluids **13**, 997 (2001).

[35] B. Shotorban and F. Mashayek, Modeling subgrid-scale effects on particles by approximate deconvolution, Phys. Fluids **17**, 081701 (2005).

[36] Q. Wang and K. D. Squires, Large eddy simulation of particle laden turbulent channel flow, Phys. Fluids **8**, 1207 (1996).

[37] V. Armenio, U. Piomelli, and V. Fiorotto, Effect of the subgrid scales on particle motion, Phys. Fluids **11**, 3030 (1999).

[38] M. Cernick, Particle subgrid scale modeling in large-eddy simulation of particle-laden turbulence, Ph.D. thesis, McMaster University, 2013.

[39] C. Marchioli, Large-eddy simulation of turbulent dispersed flows: A review of modelling approaches, Acta Mech. **228**, 741 (2017).

[40] Q. Wang and K. Squires, Large eddy simulation of particle deposition in a vertical turbulent channel flow, Int. J. Multiphase Flow **22**, 667 (1996).

[41] G. I. Park, M. Bassenne, J. Urzay, and P. Moin, A simple dynamic subgrid-scale model for les of particle-laden turbulence, Phys. Rev. Fluids **2**, 044301 (2017).

[42] M. Salmanzadeh, M. Rahnama, and G. Ahmadi, Effect of sub-grid scales on large eddy simulation of particle deposition in a turbulent channel flow, Aerosol Sci. Technol. **44**, 796 (2010).

[43] B. Shotorban and F. Mashayek, A stochastic model for particle motion in large-eddy simulation, J. Turbul. **7**, N18 (2006).

[44] B. Ray and L. R. Collins, A subgrid model for clustering of high-inertia particles in large-eddy simulations of turbulence, J. Turbul. **15**, 366 (2014).

[45] J. G. Kuerten, Point-particle DNS and LES of particle-laden turbulent flow: A state-of-the-art review, Flow, Turbul. Combust. **97**, 689 (2016).

[46] F. Battista, J.-P. Mollicone, P. Gualtieri, R. Messina, and C. M. Casciola, Exact regularised point particle (ERPP) method for particle-laden wall-bounded flows in the two-way coupling regime, J. Fluid Mech. **878**, 420 (2019).

[47] P. Gualtieri, F. Picano, G. Sardina, and C. M. Casciola, Exact regularized point particle method for multiphase flows in the two-way coupling regime, J. Fluid Mech. **773**, 520 (2015).

[48] H. Nasr and G. Ahmadi, The effect of two-way coupling and inter-particle collisions on turbulence modulation in a vertical channel flow, Int. J. Heat Fluid Flow **28**, 1507 (2007).

[49] G. Wang, K. O. Fong, F. Coletti, J. Capecelatro, and D. H. Richter, Inertial particle velocity and distribution in vertical turbulent channel flow: A numerical and experimental comparison, Int. J. Multiphase Flow **120**, 103105 (2019).

[50] C. Peng, O. M. Ayala, and L.-P. Wang, A direct numerical investigation of two-way interactions in a particle-laden turbulent channel flow, J. Fluid Mech. **875**, 1096 (2019).

[51] R. Gore and C. Crowe, Effect of particle size on modulating turbulent intensity, Int. J. Multiphase Flow **15**, 279 (1989).

[52] T. Tanaka and J. K. Eaton, Classification of Turbulence Modification by Dispersed Spheres Using a Novel Dimensionless Number, Phys. Rev. Lett. **101**, 114502 (2008).

[53] A. Soldati and C. Marchioli, Sediment transport in steady turbulent boundary layers: Potentials, limitations, and perspectives for Lagrangian tracking in DNS and LES, Adv. Water Resour. **48**, 18 (2012).

[54] H. Eckelmann, The structure of the viscous sublayer and the adjacent wall region in a turbulent channel flow, J. Fluid Mech. **65**, 439 (1974).

[55] R. D. Moser, J. Kim, and N. N. Mansour, Direct numerical simulation of turbulent channel flow up to $Re\tau = 590$, Phys. Fluids **11**, 943 (1999).

[56] S. B. Pope, *Turbulent Flows* (Cambridge University Press, Cambridge, 2000).

[57] M. Germano, U. Piomelli, P. Moin, and W. H. Cabot, A dynamic subgrid-scale eddy viscosity model, Phys. Fluids **3**, 1760 (1991).

[58] E. Pomraning and C. J. Rutland, Dynamic one-equation nonviscosity large-eddy simulation model, AIAA J. **40**, 689 (2002).

[59] L. Schiller, A drag coefficient correlation, Zeit. Ver. Deutsch. Ing. **77**, 318 (1933).

[60] P. Gualtieri, F. Picano, G. Sardina, and C. M. Casciola, Clustering and turbulence modulation in particle-laden shear flows, J. Fluid Mech. **715**, 134 (2013).

[61] C. D. Dritselis and N. S. Vlachos, Large eddy simulation of gas-particle turbulent channel flow with momentum exchange between the phases, Int. J. Multiphase Flow **37**, 706 (2011).